ChemPubSoc Europe

DOI: 10.1002/chem.201600109

CHEMISTRY
A European Journal
Full Paper

Covalent Organic Frameworks

Bimodal Functionality in a Porous Covalent Triazine Framework by Rational Integration of an Electron-Rich and -Deficient Pore Surface

Avishek Karmakar,[a] Amrit Kumar,[a] Abhijeet K. Chaudhari,[a] Partha Samanta,[a] Aamod V. Desai,[a] Rajamani Krishna,[b] and Sujit K. Ghosh*[a]

Abstract: A porous covalent triazine framework (CTF) consisting of both an electron-deficient central triazine core and electron-rich aromatic building blocks is reported. Taking advantage of the dual nature of the pore surface, bimodal functionality has been achieved. The electron deficiency in the central core has been utilized to address one of the pertinent problems in chemical industries, namely separation of benzene from its cyclic saturated congener, that is, cyclohexane. Also, by virtue of the electron-rich aromatic rings with Lewis basic sites, aqueous-phase chemical sensing of a nitroaromatic compound of highly explosive nature (2,4,6-trinitrophenol; TNP) has been achieved. The present compound supersedes the performance of previously reported COFs in both the aspects. Notably, this reports the first example of pore-surface engineering leading to bimodal functionality in CTFs.

Introduction

The development of multifunctional materials has been a theme of cutting-edge research in this changing world. Since the dawn of the age of industries, development of cheap materials with multiple functionalities which can be produced in a bulk scale and therefore be utilized in intensive industries, is an imperative issue. Various materials have been have been tried and tested by the people in both industries and academia to integrate multifunctional character in the same material.[1] Metal–organic frameworks (MOFs), which belong to the porous materials domain, are one such class of multifunctional materials which have been well-known for their plethoric applications in almost all spheres ranging from gas storage, separations, to more recent applications in clean-energy and fuel-cell applications.[2] Recently a new class of similar porous materials, known as covalent-organic frameworks (COFs), have been introduced, which are a unique class of crystalline organic polymers with extended porous ordered structures built from pre-designed simple organic motifs.[3] Owing to the lightweight composition of these materials, COFs have low mass densities and possess considerable porosity.[4] Covalent triazine frameworks (CTFs) are an important subclass of COFs that have been known for their chemical and thermal stability.[5] The ease of syntheses by simple acid-catalysed room-temperature reaction allows an added advantage in the synthetic procedures. Pre-designing CTF in view of specific functionalities is desired because of growing demand of incorporating multifarious functionalities in the same material. For example, simultaneous incorporation of both electron-rich and electron-deficient functionalities in the CTF material would pave way for fabrication of dual-functionalized pore surface. The central triazine ring in CTF formed by cyclotrimerisation reaction of the C≡N bonds renders an inherent electron deficiency to framework. Likewise, if electron rich aromatic building blocks with Lewis basic sites can utilized to constitute a CTF, then applications related to both electron deficient and/or rich pore surfaces can be achieved strategically (Scheme 1).

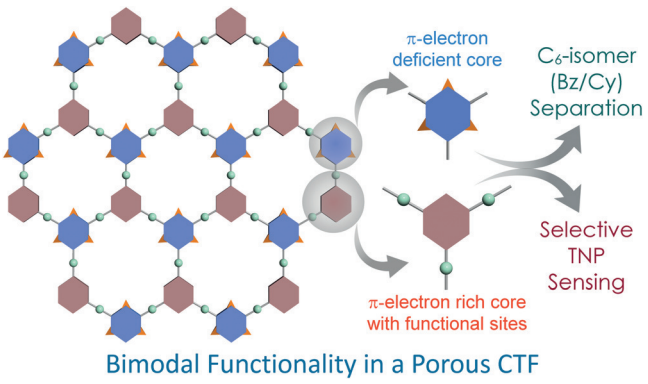

Scheme 1. Representation of the bimodal functionality in CTF-IP10 by virtue of the electron-deficient and electron-rich pore surface.

[a] A. Karmakar, A. Kumar, A. K. Chaudhari, P. Samanta, A. V. Desai, Dr. S. K. Ghosh
Department of Chemistry, Indian Institute of Science Education and Research (IISER) Pune
Dr. Homi Bhabha Road, Pashan, Pune 411008 (India)
E-mail: sghosh@iiserpune.ac.in
Homepage: http://www.iiserpune.ac.in/~sghosh/

[b] R. Krishna
University of Amsterdam (the Netherlands)

Supporting information and the ORCID identification number(s) for the author(s) of this article can be found under http://dx.doi.org/10.1002/chem.201600109.

Owing to the paucity in the electronic cloud centrally, CTFs can serve as a selective adsorbent for electron-rich aromatic molecules.[6] The differential electronic attraction of CTFs towards two molecules of similar sizes but different electron densities such as benzene and cyclohexane may result in separation of these two C_6 cyclic congeners. Separation of benzene/cyclohexane is of paramount importance because benzene in its pure form is one of the vital building blocks in chemical industries, with a production of about 43.7 metric tonnes annually.[7] Cyclohexane, which is a by-product of the hydrogenation of benzene, impedes in separation-based industries because of the closeness in the physical properties with benzene (Table S1 in the Supporting Information). CTFs, by the virtue of its large porous nature and electron-deficient pore surface, can act as a selective adsorbent for benzene molecules and separate it from cyclohexane by a much less energy/cost-demanding adsorption process. On the other hand, it is well known that molecules comprised of electron-rich substituents or functional organic sites can sense electron-deficient nitroaromatic compounds (NACs).[8] NACs are the key constituents of explosives that are used worldwide. Among them, TNP is a renowned explosive that not only poses a threat to security, but is also known to be an environmental pollutant.[9] Considering its uses in intensive chemical industries, TNP causes unavoidable contamination in ground waters and soil. Therefore detection of even trace amount of TNP is crucial in view of the catastrophic effects it causes to the environment. Fluorometric methods of detection of TNP are known for the ease of handling procedures and the very low detection level measurements.[10] Considering the electron-deficient nature of most of these NACs and TNP in particular, if a luminescent CTF with incorporated electron-rich substituent can be designed then an efficient sensor for trace amount NACs detection can be fabricated. Considering the high chemical and thermal stability of CTF-based materials, aqueous-phase detection by fluorometric methods would serve as an added advantage in prompt detection of TNP or other NACs.

Herein, we present a new porous covalently linked triazine-based framework (CTF-IP10), built from a tripodal cyano-based monomer. The CTF owing to the electron deficiency of the triazine rings in the core shows a selective uptake of π-electron-rich unsaturated moiety (benzene) over its saturated congener (cyclohexane). Moreover, the CTF has ethereal linkage that connects the aromatic benzene rings that not only makes the CTF electron-rich but also indulges in specific hydrogen-bonding interaction resulting in chemical sensing of a NAC, namely TNP. The very high degree of quenching specifically for TNP even in concurrent presence of other nitro analytes. Although multifunctionality in porous frameworks like MOFs and zeolites are well-known, pore surface engineering resulting in bimodal functionality in the CTFs is not reported till date.

Results and Discussion

CTF-IP10 was prepared in good yield by acid-catalysed room temperature reaction of a tricyanomonomer (PCN-M1) in $CHCl_3$ as a solvent (Figure 1; see the Supporting Information for full details). The formation of the polymeric trimerised compound was monitored by IR spectra of the product. The IR spectra of the PCN-M1 and that of CTF-IP10 showed considerable difference, as the C≡N stretching frequency of the monomer at about 2300 cm^{-1} was absent in the resulting CTF, as shown in Figure 2a. Moreover the peaks characteristic of the triazine ring at about 1350 cm^{-1} and 1600 cm^{-1} appeared, indicative of the formation of the new polymeric compound. Thermogravimetric analysis of CTF-IP10 performed under N_2 atmosphere revealed very high thermal stability of more than 500 °C (Figure 2d). The thermal stability of the precursor on the other hand was much less, which is typical for a discrete organic compound. PXRD pattern of CTF-IP10 shows a peak around $2\theta = 4.8^\circ$ indicative of the crystalline nature of the polymeric framework (Figure 2c). However exact structure elucidation could not be achieved owing to absence of any long-range ordering in the bulk sample. Such type of weak crystalline nature is often observed in CTFs prepared by a room-temperature method.

The ^{13}C solid-state NMR spectra shows peak for the triazine ring carbon atoms around 170 ppm and other peaks between $\delta = 90$–200 ppm, which corresponds to other aromatic carbon atoms (Figure 2b). The solid-state field emission scanning electron microscopy (FE-SEM) images show assemblage of particles of CTF-IP10 resulting forming a sheet-like structure (Figure S4

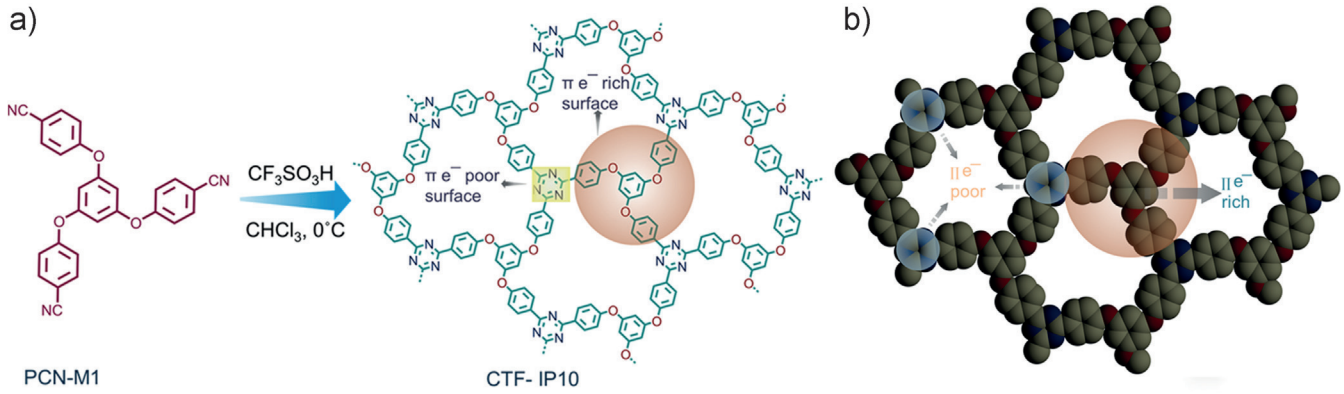

Figure 1. a) Representation of the formation of CTF-IP10 and b) space-filling diagram of a single net of CTF-IP10 showing electron-rich and electron-deficient units.

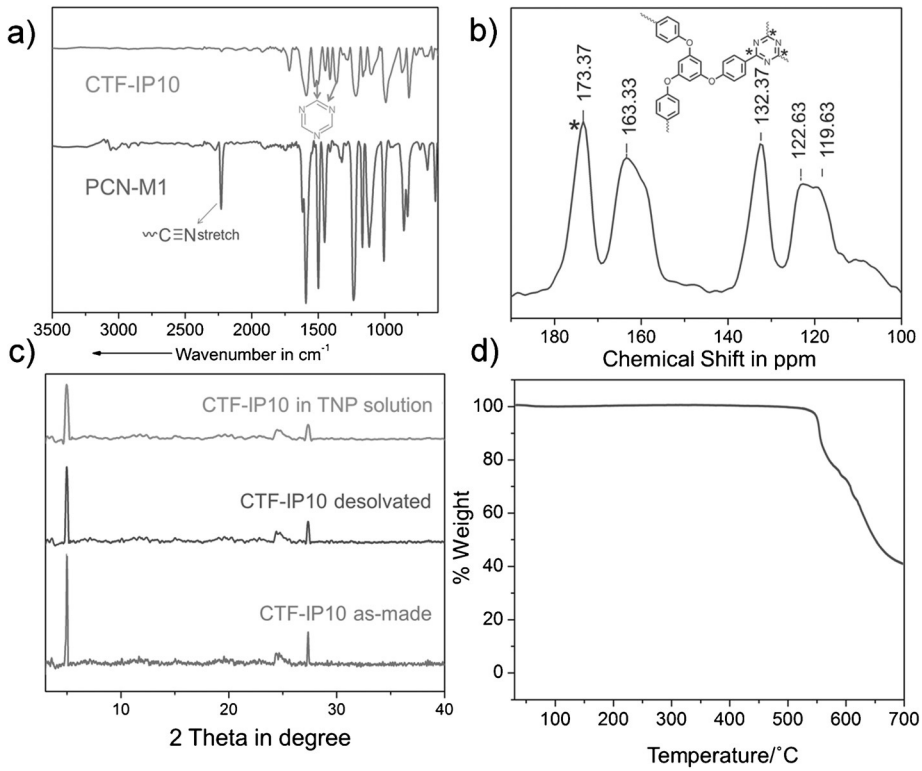

Figure 2. a) IR spectra of PCN-M1 and that of CTF-IP10 showing disappearance of the CN stretch and appearance of peaks for triazine rings in CTF-IP10. b) ^{13}C-SS-NMR for CTF-IP10. c) PXRD pattern of the CTF-IP10 compound and d) TGA profile of the desolvated phase of CTF-IP10.

in the Supporting Information). The UV/Vis solid-state reflectance spectra for PCN-M1 and the CTF compound are distinctly different owing to the increase in the conjugation, resulting in a prominent shift of around 80 nm in the CTF (Figure S3 in the Supporting Information). N_2 and CO_2 adsorption at low temperatures (77 K and 195 K, respectively) and CO_2 adsorption at 298 K (Figure 4a; Figure S5 and Figure S7 in the Supporting Information) showed sufficient porosity, which is typical for such microporous polymeric frameworks. The pore-size distribution curve shows an aperture size of 0.87 nm (Figure S8 in the Supporting Information). The Brunauer–Emmett–Teller (BET) surface area of CTF-IP10 was calculated to be 358 $m^2 g^{-1}$ and pore volume of 0.2207 $cm^3 g^{-1}$. In view of the intrinsic electron deficiency and the highly porous nature of CTF-IP10, as also evident from the DFT calculations, by mapping the electron potential of the repeating unit (Figure 3), as calculated with the Gaussian 09 Rev D program suite using DFT (structure optimized by density functional theory at the B3LYP/6-31G* level), benzene vapour adsorption was carried out at 298 K using the desolvated compound to check its response towards π-electron-rich guest molecules.

As anticipated, benzene adsorption showed a very high uptake of about 12.43 mol kg^{-1}, whereas the saturated cyclic congener (cyclohexane) measurement showed negligible uptake (Figure 4). The reason is attributed to the very strong interaction between the electron-rich benzene molecules and the π-electron-deficient triazine ring of CTF-IP10. It is hypothesized that the porous framework containing electron-deficient motifs undergo a stacking interaction with the incoming benzene molecules, thereby acting as an efficient adsorbent for benzene molecules. TGA analysis of CTF-IP10 exposed to vapours of 1:1 benzene/cyclohexane shows a steady loss corresponding to the adsorbed benzene vapours inside the porous framework. A similar exposure to pure cyclohexane solvent showed no such loss validating the fact that only benzene could be adsorbed selectively (Figure S11, S12 in the Supporting Information). UV/Vis reflectance spectra of the sample exposed to benzene vapour showed a prominent shift with respect to CTF-IP10; however, samples exposed to cyclohexane vapour showed no such striking shift in the wavelength (Figure S13 in the Supporting Information). All of these results prove that that benzene is selectively adsorbed by CTF-IP10

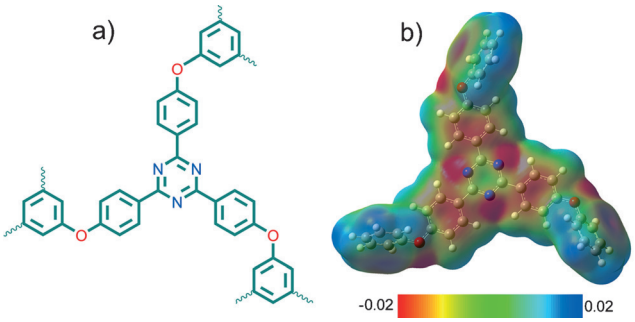

Figure 3. a) Structure of the repeating unit of CTF-IP10 and b) electronic potential map of the repeating unit showing the electron-deficient and -rich surface.

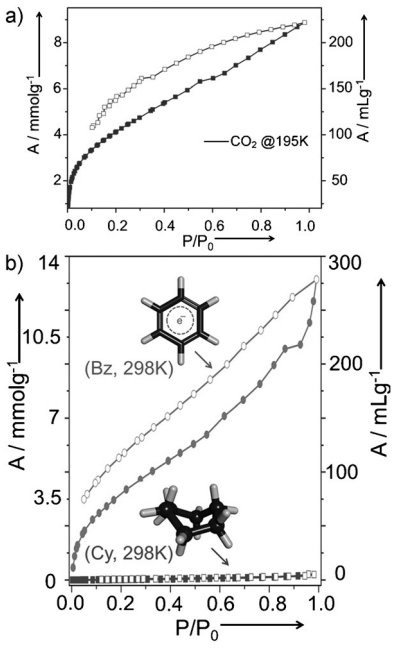

Figure 4. Top: CO_2 adsorption isotherm of CTF-IP10 at 195 K. Bottom: benzene adsorption (●, ○) and cyclohexane adsorption (■, □) at 298 K.

both from the perspective of the single component adsorption isotherm and also from binary mixtures of both benzene and cyclohexane. Such a targeted syntheses of CTF for selective adsorption of benzene makes it act as selective molecular sponge for benzene molecule. To further study in detail, we evaluated Bz/Cy separation by utilizing the ideal adsorbed solution theory (IAST) calculations. Figure 5a shows the experimental data for pure component isotherms for benzene and cyclohexane in CTF-IP10; the continuous solid lines are Langmuir–Freundlich fits; the parameters are specified in Table S2 in the Supporting Information. For fitting purposes, only the adsorption branches of the isotherms were considered. IAST calculations for benzene uptake capacity for equimolar benzene/cyclohexane mixtures in CTF-IP10 showed that for pressures exceeding about 1 kPa, the adsorbed phase contain predominantly benzene; this indicates good separation characteristics, as shown in Figure 5b. Figure 5c shows IAST calculations for adsorption selectivity, S_{ads}, for equimolar benzene/cyclohexane mixtures. We note that the value of S_{ads} for CTF-IP10 is in excess of about 50. In view of the significantly higher uptake capacity of benzene in CTF-IP10, we should expect that the separation performance of benzene/cyclohexane mixtures with CTF-IP10 would be significantly higher than that of DAT-MOF-1, the separations of which were reported in our earlier work.[11] Breakthrough simulations, carried out with the method described in our earlier work,[12] show that clear separations of equimolar benzene/cyclohexane mixtures are achievable with CTF-IP10; see Figure 5d. A video animation (see the Supporting Information) demonstrates the superior selective adsorption ability of CTF-IP10 for benzene over cyclohexane.

In our endeavour to exploit effect of electron-rich building units on electron-deficient NACs, a fluorometric detection

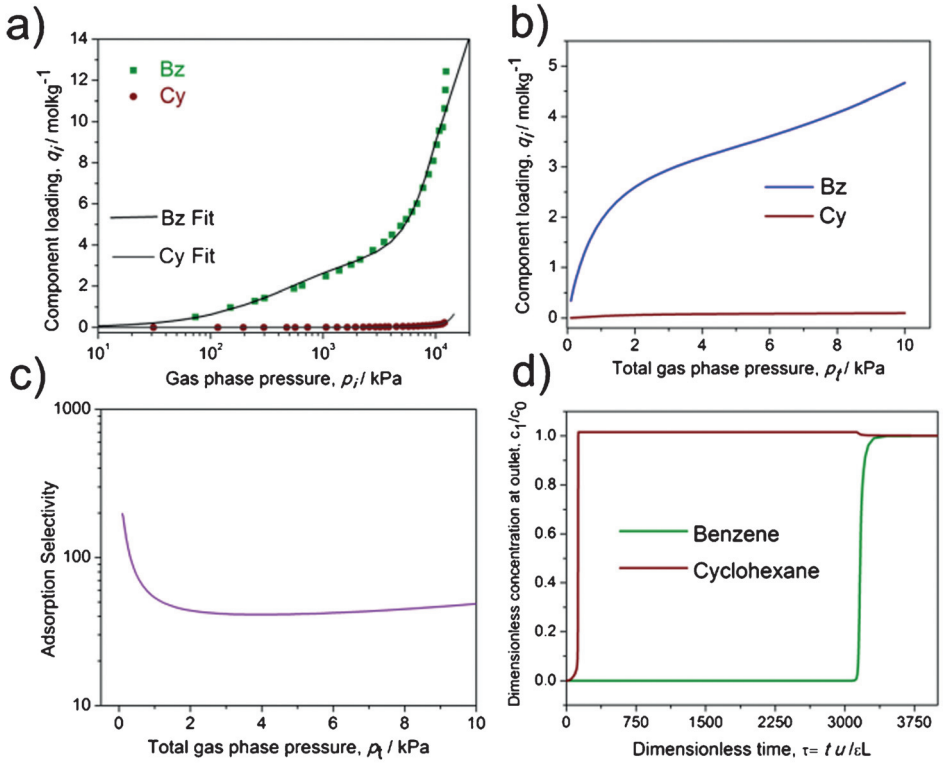

Figure 5. a) Experimental data for pure component isotherms for benzene and cyclohexane in CTFIP-10; the continuous solid lines are Langmuir–Freundlich fits. b) IAST calculations for benzene uptake capacity for equimolar benzene/cyclohexane mixtures in CTFIP-10. c) IAST calculations for adsorption selectivity, for equimolar benzene/cyclohexane mixtures by CTF-IP10. d) Breakthrough simulations for Bz/Cy in a fixed bed of CTF-IP10 at 298 K.

study was carried out in disperse phase with the aquatically stable fluorescent CTF-IP10. In a typical experiment, 2 mg of the solid sample was dispersed in 1:0.25 mixture of H_2O/EtOH and incremental addition from a stock solution of 1 mmol nitrobenzene (NB), 2,4-dinitrotoluene (2,4-DNT), 2,6-dinitrotoluene (2,6-DNT), 2,4,6-trinitrotoluene (TNT), 2,4,6-trinitrophenol (TNP), and 1,3,5-trinitroperhydro-1,3,5-triazine (RDX) in 5 mL of water was carried out. When excited at around 340 nm (Figure S14 in the Supporting Information), other nitroanalytes exhibited negligible to moderate quenching behaviour, whereas for TNP highest quenching effect on CTF-IP10 was observed (Figure 7a; Figures S15–S22 in the Supporting Information). About 98% fluorescence quenching was observed in the case of TNP upon addition of only 80 μL of the analyte (Figure 6).

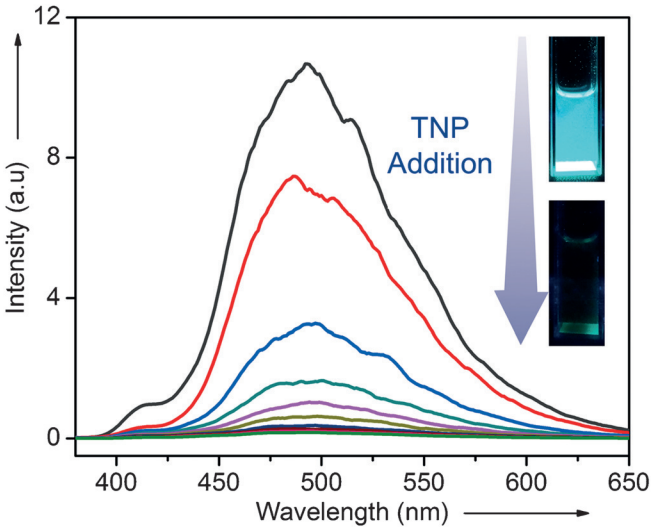

Figure 6. Fluorescence spectra of CTF-IP10 upon incremental addition of TNP in 1:0.25 mixture of H_2O/EtOH showing changes in photoluminescence under UV light.

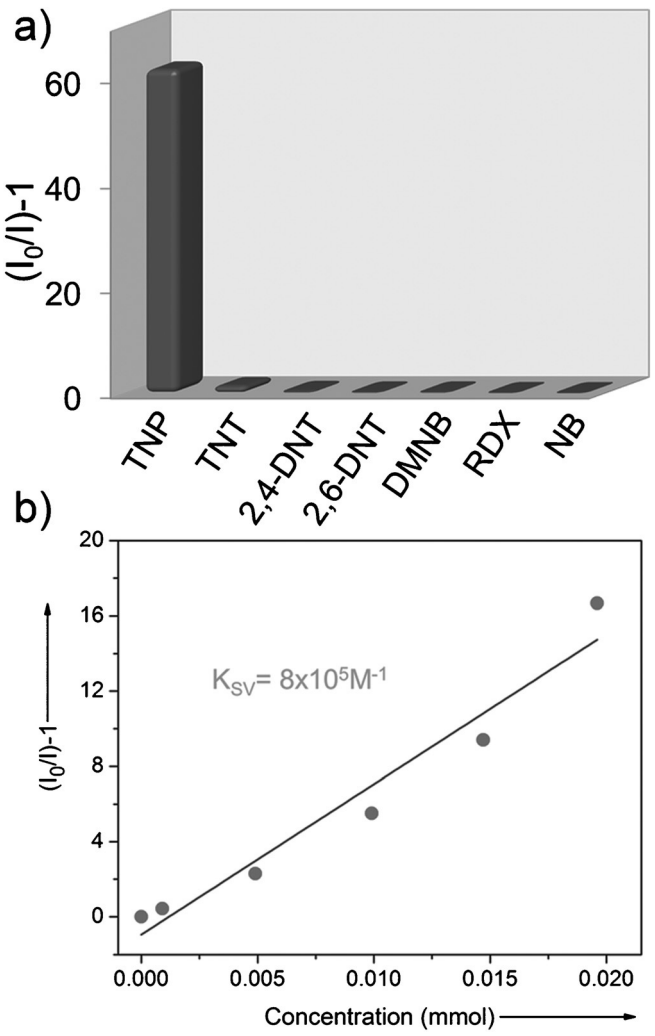

Figure 7. a) Fluorescence response of CTF-IP10 towards various nitroaromatic compounds showing maximum response towards TNP and b) SV plot of TNP titration at low concentration.

The electron-deficient TNP and other NACs can diffuse through the porous channels of the framework as a result of suitable interactions with the electron-rich substituents of CTF-IP10. Of them, TNP causes the maximum quenching effect. The quenching constant (K_{sv}) as calculated by Stern–Volmer equation showed a very high value of 8×10^5 L mol^{-1} at low concentration (Figure 7b), which is one of the highest known K_{sv} value for TNP in the COF regime. Encouraged by the above result, a competitive assay was performed to check whether the efficiency of quenching was consistent in presence of other competing nitro analytes. In a systematically designed experimental procedure, other competing analytes were added to CTF-IP10 and fluorescence spectra were recorded. A little change in fluorescence intensity was observed as compared to the parent compound. However, when TNP was added to the same solution, a sharp decrease in fluorescence intensity was observed. This cycle was repeated for three consecutive times and consistent results were observed (FigureS25 in the Supporting Information). Thus the efficacy of CTF-IP10 towards selective sensing of TNP was unaffected even in multicomponent mixtures of other analytes. This showed that even in concurrent presence of other nitroanalytes, the CTF-IP10 showed a far superior response towards TNP. The stability of CTF-IP10 in TNP was checked by dipping the desolvated compound in TNP solution for about 10 days, after which PXRD was recorded. The CTF showed retention in crystallinity confirming the high chemical stability of the present compound. To investigate the mechanism of quenching, we turned to calculate the HOMO–LUMO energies for the nitro analytes by DFT by using the B3LYP/6-31G* method with Gaussian 09 package. The LUMO orbitals of TNP are the lowest-lying (Figure 8), which is indicative of the fact that very fast and efficient photoinduced electron transfer may occur from the π orbitals of the electron-rich components of CTF-IP10, that is, the phenyl rings with ethereal linkage. TNP, being the most electron-deficient species, readily accepts the electron from the HOMO orbital of the donor, resulting in significant fluorescence quenching.

To validate the mechanism of the electron donation from the conduction band of the CTF to the LUMO of the analyte, a control experiment in which other phenol derivatives, such

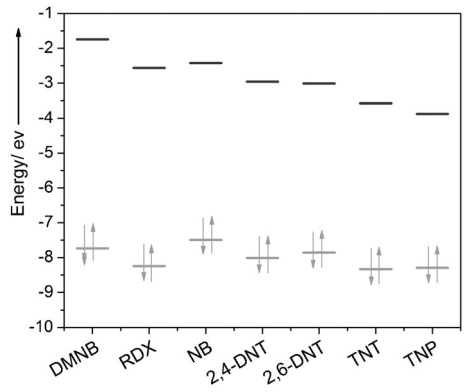

Figure 8. HOMO and LUMO energies of electron-deficient nitro analytes calculated by DFT.

as nitrophenol and 2,4-dinitrophenol, were titrated to observe the quenching behaviour. As expected the percentage quenching values were significantly lower compared to TNP (32% for NP and 56% for 2,4-DNP; Figure S24 in the Supporting Information). The trend follows the exact order of electron deficiency in such nitrophenols. TNP, being the most electron-deficient among the three owing to the presence of three electron-withdrawing $-NO_2$ groups, interacts significantly with the electron-rich π-orbitals of CTF-IP10, resulting in a prompt quenching response. Also the absorption spectra of TNP showed a considerable overlap with the emission spectra of the CTF-IP10 as compared to other non-emissive analytes, correlating with the fact that an energy-transfer process is also responsible for the quenching mechanism (Figure S26 in the Supporting Information). The possibility of a hydrogen-bonding interaction of the ether oxygen and/or basic nitrogen atoms of the triazine ring of the compound with the acidic phenolic hydrogen of TNP may also result in significant host–guest complexation, resulting in such effective and interesting fluorescence response. To rule out the effect of self-absorption of TNP, we performed fluorescence measurement at different excitation wavelengths ($\lambda_{exc} = 360$ nm, 390 nm and 400 nm) upon addition of TNP solution to CTF-IP10. As evident from the fluorescence profile (Figure S27 in the Supporting Information), negligible quenching was observed. The above observation also corroborated the high K_{sv} value for TNP at low concentrations. However, a non-linearity in the Stern–Volmer curve was observed indicative of both static and dynamic energy transfer mechanism occurring herein.

Conclusion

In conclusion, we have successfully employed a strategy of pore-surface engineering to achieve bimodal functionality in a porous covalent triazine framework. The combination of both electron-rich and electron-deficient building blocks in the present compound have been strategically exploited in addressing two issues of great concern, namely aqueous-phase detection of a compound of highly explosive nature (TNP) and separation of benzene molecules from its saturated congener (cyclohexane). Notably, the performance of the present compound in both the aspects supersedes both the sensing efficiency of TNP and selectivity towards benzene reported by previously reported CTFs. Pre-designing CTFs for specific functionalities in a targeted fashion can thus open up new avenues to develop multifunctional materials, to which significant attention is currently being given.

Experimental Section

PCN-M1 was synthesized according to the previously reported procedure with slight modification. All other reagents and solvents were commercially available and used without further purification. The X-ray powder pattern was recorded on a Bruker D8 Advanced X-ray diffractometer at room temperature using Cu Kα radiation ($\lambda = 1.5406$ Å). FTIR spectra were measured on NICOLET 6700 FT-IR Spectrophotometer using KBr Pellets. Thermogravimetric analyses was obtained in the temperature range of 30–800 °C on PerkinElmer STA 6000 analyser under a N_2 atmosphere at a heating rate of 10 °C min. All fluorescence measurements were done on JobinYvon Fluoroax-4 spectro fluorometer. ^1H and ^{13}C NMR was recorded in 400 MHz Jeol ECS-400 Instrument. The UV/Vis measurements were performed using Chemito SPECTRASCAN UV-2600.

Synthesis of PCN-M1: In a 50 mL flask, phloroglucinol (1 mmol) and K_2CO_3 (4.5 mmol) were suspended in DMF (10 mL). The suspension was heated at reflux temperature for 4 h. Then the reaction mixture was cooled to about 60 °C and *p*-fluorobenzonitrile (3.2 mmol) was added and heating continued at 150 °C for 24 h. On cooling, the reaction mixture was poured into 500 mL of water and the precipitated solid was collected and washed with water followed by methanol. The yield of the product was 86%. The crude product was purified by recrystallization from ethanol to afford pure compound PCN-M1.

Synthesis of CTF-IP10: Trifluoromethanesulfonic acid (0.6 g, 4 mmol) and $CHCl_3$ (10 mL) were charged into a pre-dried two-neck round-bottom flask under an N_2 atmosphere. The mixture was cooled to 0 °C and PCN-M1 (0.430 g, 1 mmol) in $CHCl_3$ (80 mL) was added into the solution dropwise over 30 min. The mixture was stirred at 0 °C for another 2 h before left overnight at room temperature. The solution turned red and solid precipitates were formed. Then, the mixture was poured into water (200 mL) containing ammonia solution (10 mL, 0.6 mmol) and stirred for 2 h. The precipitates were filtered and washed with water, ethanol, acetone, and chloroform successively. CTF-IP10 (1.1 g, 86% yield) was obtained as a light-yellow solid. Elemental analysis (%) of CTF-IP10: found: C 67.53, H 3.41, N 10.66.

Acknowledgements

P.S. is thankful to UGC for research fellowship. Av.K. and A.V.D. are thankful to IISERPune for research fellowship. We are grateful to IISER Pune for research facilities. DST (Project No. GAP/DST/CHE-12-0083) is acknowledged for the financial support.

Keywords: bimodal functionality · covalent organic frameworks · sensing · separation · triazine

[1] a) L. Nicole, L. Rozes, C. Sanchez, *Adv. Mater.* **2010**, *22*, 3208–3214; b) P. Pachfule, M. K. Panda, S. Kandambeth, S. M. Shivaprasad, D. D. Diaz, R. Banerjee, *J. Mater. Chem. A* **2014**, *2*, 7944–7952; c) K. Salonitis, J. Pandremenos, J. Paralikas, G. Chryssolouris, *Int. J. Adv. Manuf. Technol.* **2010**,

49, 803 – 826; d) Z. Guo, R. Cao, X. Wang, H. Li, W. Yuan, G. Wang, H. Wu, J. Li, *J. Am. Chem. Soc.* **2009**, *131*, 6894 – 6895; e) Q. R. Fang, G. S. Zhu, Z. Jin, M. Xue, X. Wei, D. Wang, S. L. Qiu, *Angew. Chem. Int. Ed.* **2006**, *45*, 6126 – 6130; *Angew. Chem.* **2006**, *118*, 6272 – 6276; f) D. Kubo, K. Tadanaga, A. Hayashi, M. Tatsumisago, *J. Mater. Chem. A J. Mater.Chem. A* **2013**, *1*, 6804 – 6809; g) M. Liong, J. Lu, M. Kovochich, T. Xia, S. G. Ruehm, A. E. Nel, F. Tamanoi, J. I. Zink, *ACS Nano* **2008**, *2*, 889 – 896; h) A. Corma, U. Díaz, T. García, G. Sastre, A. Velty, *J. Am. Chem. Soc.* **2010**, *132*, 15011 – 15021.

[2] a) B. Zheng, J. Bai, J. Duan, L. Wojtas, M. J. Zaworotko, *J. Am. Chem. Soc.* **2011**, *133*, 748 – 751; b) K. Li, D. H. Olson, J. Y. Lee, W. Bi, K. Wu, T. Yuen, Q. Xu, J. Li, *Adv. Funct. Mater.* **2008**, *18*, 2205 – 2214; c) T. K. Maji, R. Matsuda, S. Kitagawa, *Nat. Mater.* **2007**, *6*, 142 – 148; d) J. A. Hurd, R. Vaidhyanathan, V. Thangadurai, C. I. Ratcliffe, I. L. Moudrakovski, G. K. H. Shimizu, *Nat. Chem.* **2009**, *1*, 705 – 710; e) J. Yu, Y. Cui, C. Wu, Y. Yang, B. Chen, G. Qian, *J. Am. Chem. Soc.* **2015**, *137*, 4026 – 4029; f) S. Y. Zhang, L. Wojtas, M. J. Zaworotko, *J. Am. Chem. Soc.* **2015**, *137*, 12045 – 12049; g) M. Inukai, S. Horike, W. Chen, D. Umeyama, T. Itakura, S. Kitagawa, *J. Mater. Chem. A* **2014**, *2*, 10404 – 10409; h) K. Tan, S. Zuluaga, Q. Gong, Y, Gao, N. Nijem, J. Li, T. Thonhauser, Y. J. Chabal, *Chem. Mater.* **2015**, *27*, 2203 – 2217; i) H. C. Zhou, S. Kitagawa, *Chem. Soc. Rev.* **2014**, *43*, 5415 – 5418; j) M. S. Denny Jr, S. M. Cohen, *Angew. Chem. Int. Ed.* **2015**, *54*, 9029 – 9032; *Angew. Chem.* **2015**, *127*, 9157 – 9160; k) D. Zhao, D. Yuan, H. C. Zhou, *Energy Environ. Sci.* **2008**, *1*, 222 – 235.

[3] a) X. Feng, X. Ding, D. Jiang, *Chem. Soc. Rev.* **2012**, *41*, 6010 – 6022; b) H. Furukawa, O. M. Yaghi, *J. Am. Chem. Soc.* **2009**, *131*, 8875 – 8883; c) A. P. Côté, A. I. Benin, N. W. Ockwig, M. O'Keeffe, A. J. Matzger, O. M. Yaghi, *Science* **2007**, *316*, 268 – 272; d) S. Wan, J. Guo, J. Kim, H. L. Ihee, D. Jiang, *Angew. Chem. Int. Ed.* **2008**, *47*, 8826 – 8830; *Angew. Chem.* **2008**, *120*, 8958 – 8962; e) E. L. Spitler, W. R. Dichtel, *Nat. Chem.* **2010**, *2*, 672 – 677; f) H. Xu, J. Gao, D. Jiang, *Nat. Chem.* **2015**, *7*, 905 – 912.

[4] a) D. Yuan, W. Lu, D. Zhao, H. C. Zhou, *Adv. Mater.* **2011**, *23*, 3723 – 3725; b) A. Nagai, X. Chen, X. Feng, X. Ding, Z. Guo, D. Jiang, *Angew. Chem. Int. Ed.* **2013**, *52*, 3770 – 3774; *Angew. Chem.* **2013**, *125*, 3858 – 3862; c) H. A. Patel, S. H. Je, J. Park, D. P. Chen, Y. Jung, C. T. Yavuz, A. Coskun, *Nat. Commun.* **2013**, DOI: 10.1038/ncomms2359; d) S. B. Kalidindi, C. Wiktor, A. Ramakrishnan, J. Webing, A. Schneemann, G. Van Tendeloo, R. A. Fischer, *Chem. Commun.* **2013**, *49*, 463 – 465; e) S. Y. Ding, W. Wang, *Chem. Soc. Rev.* **2013**, *42*, 548 – 568; f) S. L. Cai, Y. B. Zhang, A. B. Pun, B. He, J. Yang, F. M. Toma, I. D. Sharp, O. M. Yaghi, J. Fan, S. R. Zheng, W.-G. Zhang, Y. Liu, *Chem. Sci.* **2014**, *5*, 4693 – 4700; g) Y. B. Zhang, J. Su, H. Furukawa, Y. Yun, F. Gándara, A. Duong, X. Zou, O. M. Yaghi, *J. Am. Chem. Soc.* **2013**, *135*, 16336 – 16339; h) J. Thote, H. B. Aiyappa, A. Deshpande, D. D. Díaz, S. Kurungot, R. Banerjee, *Chem. Eur. J.* **2014**, *20*, 15961 – 15965; i) D. D. Medina, J. M. Rotter, Y. Hu, M. Dogru, V. Werner, F. Auras, J. T. Markiewicz, P. Knochel, T. Bein, *J. Am. Chem. Soc.* **2015**, *137*, 1016 – 1019; j) N. Huang, X. Ding, J. Kim, H. Ihee, D. Jiang, *Angew. Chem. Int. Ed.* **2015**, *54*, 8704 – 8707; *Angew. Chem.* **2015**, *127*, 8828 – 8831; k) F. Xu, H. Xu, X. Chen, D. Wu, Y. Wu, H. Liu, C. Gu, R. Fu, D. Jiang, *Angew. Chem. Int. Ed.* **2015**, *54*, 6814 – 6818; *Angew. Chem.* **2015**, *127*, 6918 – 6922.

[5] a) P. Kuhn, M. Antonietti, A. Thomas, *Angew. Chem. Int. Ed.* **2008**, *47*, 3450 – 3453; *Angew. Chem.* **2008**, *120*, 3499 – 3502; b) S. Hug, M. B. Mesch, H. Oh, N. Popp, M. Hirscher, J. Senkerd, B. V. Lotsch, *J. Mater. Chem. A* **2014**, *2*, 5928 – 5936; c) X. Jiang, P. Wang, J. Zhao, *J. Mater. Chem. A* **2015**, *3*, 7750 – 7758; d) P. Kuhn, A. Forget, D. Su, A. Thomas, M. Antonietti, *J. Am. Chem. Soc.* **2008**, *130*, 13333 – 13337; e) S. Ren, M. J. Bojdys, R. Dawson, A. Laybourn, Y. Z. Khimyak, D. J. Adams, A. I. Cooper, *Adv. Mater.* **2012**, *24*, 2357 – 2361; f) X. Zhu, C. Tian, S. M. Mahurin, S. Hai Chai, C. Wang, S. Brown, G. M. Veith, H. Luo, H. Liu, S. Dai, *J. Am. Chem. Soc.* **2012**, *134*, 10478 – 10484.

[6] a) M. Mascal, A. Armstrong, M. D. Bartberger, *J. Am. Chem. Soc.* **2002**, *124*, 6274 – 6276; b) J. Liu, E. Zong, H. Fu, S. Zheng, Z. Xu, D. Zhu, *J. Colloid Interface Sci.* **2012**, *372*, 99 – 107; c) H. Ren, T. Ben, E. Wang, X. Jing, M. Xue, B. Liu, Y. Cui, S. Qiu, G. Zhu, *Chem. Commun.* **2010**, *46*, 291 – 293; d) W. Wang, P. Hobza, *ChemPhysChem* **2008**, *9*, 1003 – 1009.

[7] a) Y, Hijikata, S, Horike, M, Sugimoto, H, Sato, R. Matsuda, S. Kitagawa, *Chem. Eur. J.* DOI: 10.1002/chem.201003734; b) S. K. Gade, V. A. Tuan, C. J. Gump, R. D. Noble, J. L. Falconer, *Chem. Commun.* **2001**, 601 – 602; c) S. Shimomura, S. Horike, R. Matsuda, S. Kitagawa, *J. Am. Chem. Soc.* **2007**, *129*, 10990 – 10991; d) Y. X. Bai, J. W. Qian, Q. Zhao, Y. Xu, S. R. Ye, *J. Appl. Polym. Sci.* **2006**, *102*, 2832 – 2838; e) A. Karmakar, A. V. Desai, B. Manna, B. Joarder, S. K. Ghosh, *Chem. Eur. J.* **2015**, *21*, 7071 – 7076; f) Y. Yang, Q. Zhang, Z. Zhang, S. Zhang, *J. Mater. Chem. A* **2013**, *1*, 10368 – 10374.

[8] a) S. Pramanik, C. Zheng, X. Zhang, T. J. Emge, J. Li, *J. Am. Chem. Soc.* dx.doi.org/10.1021/ja106851d; b) D. Li, J. Liu, R. T. K. Kwok, Z. Liang, B. Z. Tang, J. Yu, *Chem. Commun.* **2012**, *48*, 7167 – 7169; c) S. S. Nagarkar, B. Joarder, A. K. Chaudhari, S. Mukherjee, S. K. Ghosh, *Angew. Chem. Int. Ed.* **2013**, *52*, 2881 – 2885; *Angew. Chem.* **2013**, *125*, 2953 – 2957; d) S. S. Nagarkar, A. V. Desai, S. K. Ghosh, *Chem. Commun.* **2014**, *50*, 8915 – 8918; e) G. Das, B. P. Biswal, S. Kandambeth, V. Venkatesh, G. Kaur, M. Addicoat, T. Heine, S. Verma, R. Banerjee, *Chem. Sci.* **2015**, *6*, 3931 – 3939.

[9] a) Y. Salinas, R. Martinez-Manez, M. D. Marcos, F. Sancenon, A. M. Castero, M. Parra, S. Gil, *Chem. Soc. Rev.* **2012**, *41*, 1261 – 1296; b) S. W. Thomas, G. D. Joly, T. M. Swager, *Chem. Soc. Rev.* **2007**, *107*, 1339; c) M. E. Germain, M. J. Knapp, *Chem. Soc. Rev.* **2009**, *38*, 2543 – 2555; d) G. He, H. Peng, T. Liu, M. Yang, Y. Zhang, Y. Fang, *J. Mater. Chem.* **2009**, *19*, 7347; e) P. G. Thorne, T. F. Jenkins, *Field Anal. Chem. Technol.* **1997**, *1*, 165 – 167; f) K. M. Wollin, H. H. Dieter, *Arch. Environ. Contam. Toxicol.* **2005**, *49*, 18 – 21.

[10] a) Y. Yuan, H. Ren, F. Sun, X. Jing, K. Cai, X. Zhao, Y. Wang, Y. Wei, G. Zhu, *J. Phys. Chem. C* **2012**, *116*, 26431 – 26435; b) S. Dalapati, S. Jin, J. Gao, Y. Xu, A. Nagai, D. Jiang, *J. Am. Chem. Soc.* **2013**, *135*, 17310 – 17313; c) D. Gopalakrishnan, W. R. Dichtel, *J. Am. Chem. Soc.* **2013**, *135*, 8357 – 8362; d) Z. Xiang, D. Cao, *Macromol. Rapid Commun.* **2012**, *33*, 1184 – 1190; e) Y. Xin, Q. Wang, T. Liu, L. Wang, J. Li, Y. Fang, *Lab Chip* **2012**, *12*, 4821; f) A. Lan, K. Li, H. Wu, D. H. Olson, T. J. Emge, W. Ki, M. Hong, J. Li, *Angew. Chem. Int. Ed.* **2009**, *48*, 2334 – 2338; *Angew. Chem.* **2009**, *121*, 2370 – 2374.

[11] B. Manna, S. Mukherjee, A. V. Desai, S. Sharma, R. Krishna, S. K. Ghosh, *Chem. Commun.* **2015**, *51*, 15386 – 15389.

[12] R. Krishna, *RSC Adv.* **2015**, *5*, 52269 – 52295.

Received: January 11, 2016
Revised: January 18, 2016
Published online on February 18, 2016

CHEMISTRY
A European Journal

Supporting Information

Bimodal Functionality in a Porous Covalent Triazine Framework by Rational Integration of an Electron-Rich and -Deficient Pore Surface

Avishek Karmakar,[a] Amrit Kumar,[a] Abhijeet K. Chaudhari,[a] Partha Samanta,[a] Aamod V. Desai,[a] Rajamani Krishna,[b] and Sujit K. Ghosh*[a]

chem_201600109_sm_miscellaneous_information.pdf

Supporting Information

Bimodal functionality in a porous covalent triazine framework by rational integration of electron rich and deficient pore surface

Avishek Karmakar,[a] Amrit Kumar,[a] Abhijeet K. Chaudhari,[a] Partha Samanta,[a] Aamod V. Desai,[a] Rajamani Krishna,[b] Sujit K. Ghosh[a]*

[a] Indian Institute of Science Education and Research (IISER), Dr. Homi Bhabha Road, Pashan, Pune-411008, India

[b] Van't Hoff Institute for Molecular Sciences, University of Amsterdam, Science Park 904, 1098 XH Amsterdam, The Netherlands

E-mail: *sghosh@iiserpune.ac.in* ***Fax:*** *+91-20-25908186* ***Tel:*** *+91-20-25908076*

Table of Contents

Experimental Section:

Caution! TNT, RDX and TNP are highly explosive and should be handled carefully and in small amounts. The explosives were handled as dilute solutions and with safety measures to avoid explosion.

Materials: TNT and RDX were obtained from HEMRL Pune (India). TNP, 2,4-DNT, 2,6-DNT, DMNB, NM were purchased from Aldrich, 1,3-DNB, NB from local company and used as received. Dry solvents were used during complete analysis and were obtained locally.

Physical Measurements: Powder X-ray diffraction patterns (PXRD) were measured on Bruker D8 Advanced X-Ray diffractometer using Cu Kα radiation (λ= 1.5406 Å) with a tube voltage of 40 kV and current of 40 mA in 5 to 40° 2θ range. Thermogravimetric analyses were recorded on Perkin-Elmer STA 6000 TGA analyzer under N_2 atmosphere with a heating rate of 10 °C min^{-1}. Fluorescence measurements were done using Horiba FluoroMax 4 with stirring attachment. ^{1}H and ^{13}C NMR was recorded in 400 MHz Jeol ECS-400 Instrument. The UV-Vis measurements were performed using Chemito SPECTRASCAN UV-2600.

Sorption Measurements: Solvent sorption measurements were performed using BelSorpmax (Bel Japan). All of the solvents used were of 99.99% purity. The desolvated sample of CTF-IP10 was obtained by heating sample at 150 °C under vacuum for 8h and the desolvation was confirmed by TGA and PXRD. Prior to adsorption measurement the desolvated sample was pre-treated at 100 °C under vacuum for 4h using BelPrepvacII and purged with N_2 on cooling.Low pressure gas sorption measurements were performed using BelSorpmax (Bel Japan). All of the gases used were of 99.999% purity.

Photophysical study

In a typical experiment, 1 mg of **CTF-IP10** was weighed and added to a cuvette containing 1:0.25 H_2O/EtOH and stirred. Upon excitation at 340 nm, the fluorescence response of **CTF-IP10** dispersed in water was measured *in situ* in the 380-700 nm

range and the corresponding fluorescence intensity was monitored . For fluorescence titration, emission was recorded upon incremental addition of freshly prepared analyte solutions (1 mM or saturated). To maintain homogeneity, the solution was stirred at a constant rate during the experiment.

Synthesis of PCN-M1: In a 50 mL flask, 1mmol of phloroglucinol and 4.5mmol of K_2CO_3 were suspended in 10mL of DMF .The suspension was heated at reflux temperature for 4 hrs. Then the reaction mixture was cooled to about 60°C and 3.2 mmol of p-fluorobenzonitrile was added and heating continued at 150°C for 24 h. On cooling, the reaction mixture was poured into 500 mL of water and the precipitated solid was collected and washed with water followed by methanol. The yield of the product was 86%. The crude product was purified by recrystallization from ethanol to afford pure compound **PCN-M1**.

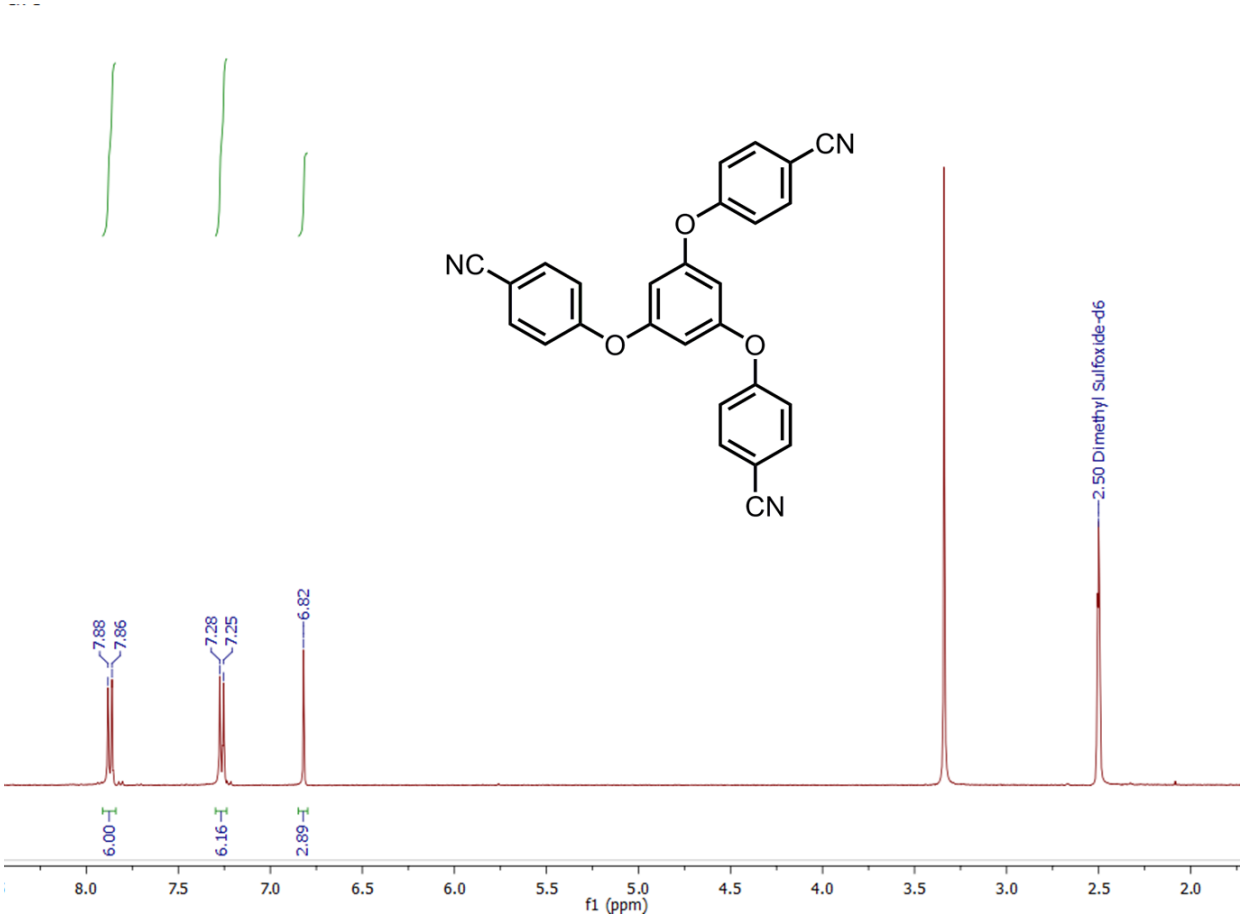

Fig.S1: ^{1}H-NMR spectrum of the **PCN-M1**.

Synthesis of CTF-IP10: Trifluoromethanesulfonic acid (.6 g, 4 mmol) and 10 mL of $CHCl_3$ were charged into a pre-dried 2-neck round bottom flask under N_2 atmosphere. The mixture was cooled to 0°C and **PCN-M1**(0.430 g, 1 mmol) in 80 mL of $CHCl_3$ was added into the solution dropwise over 30 min. The mixture was stirred at 0 °C for another 2 h before left overnight at room temperature. The solution turned red and solid precipitates were formed. Then, the mixture was poured into 200 mL of water containing 10 mL of ammonia solution and stirred for 2 h. The precipitates were filtered and washed with water, ethanol, acetone and chloroform successively. **CTF-IP10**(1.1 g, 86% yield) was obtained as a light yellow solid. Elemental analysis of CTF-IP10(%) :found: C 67.53, H 3.41, N 10.66.

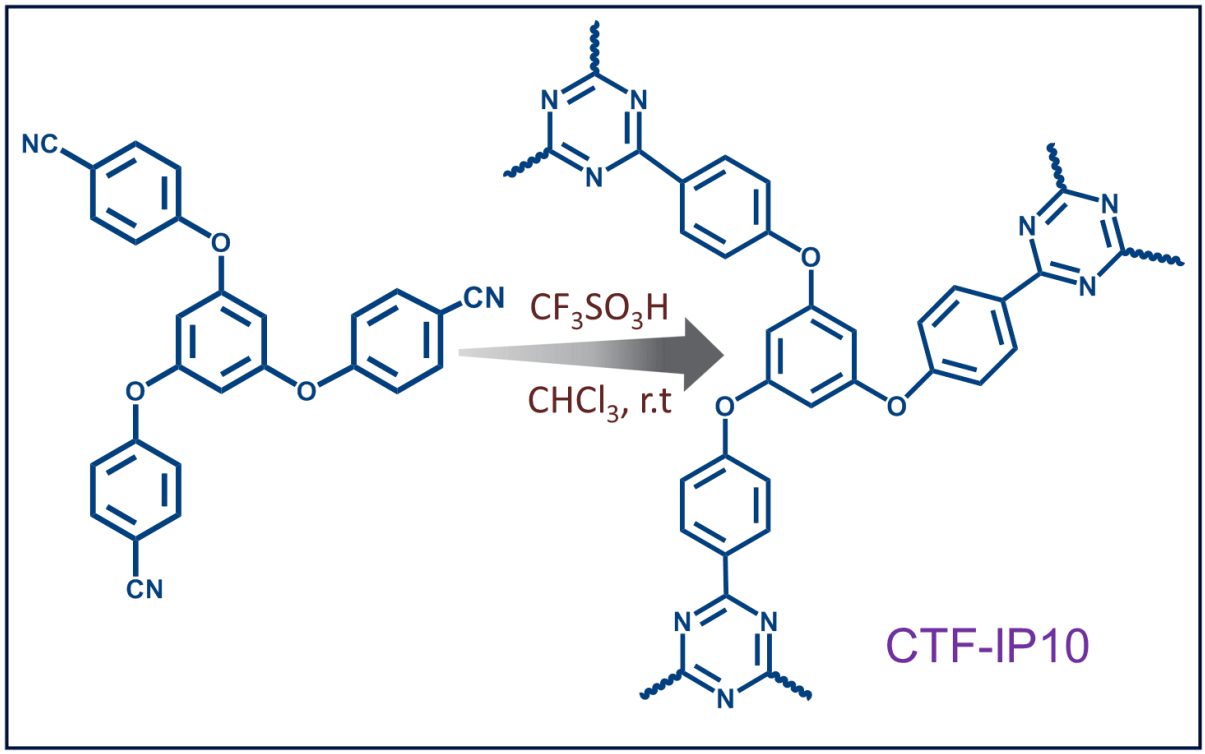

Scheme 1: Schematic representation of the synthesis of **CTF-IP10.**

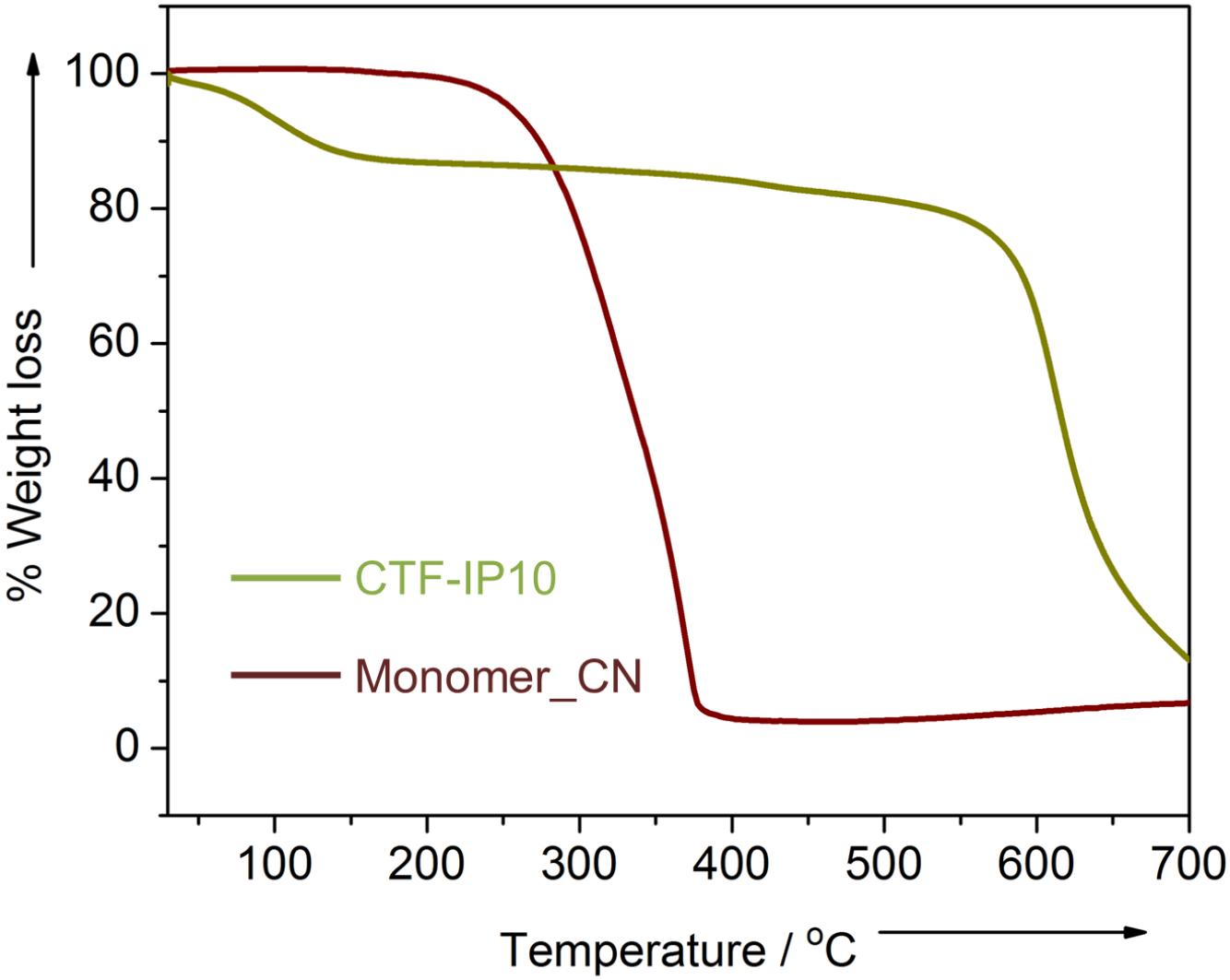

Figure S2: TGA curve of the PCN-M1 (wine red) and that of CTF-IP10;assynthesized (dark yellow).

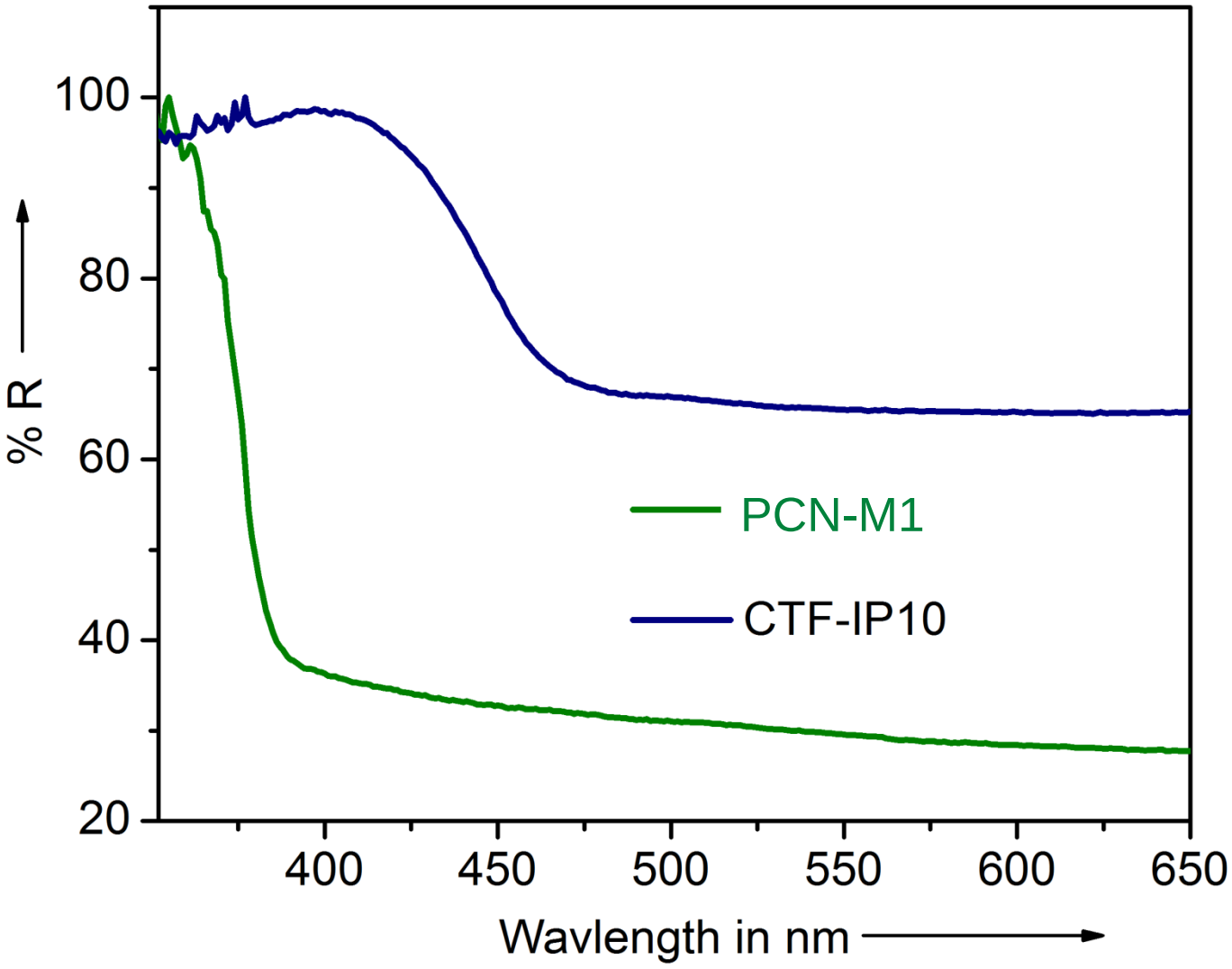

Figure S3: Solid state UV-Vis spectra of PCN-M1 (green) and CTF-IP10 (blue).

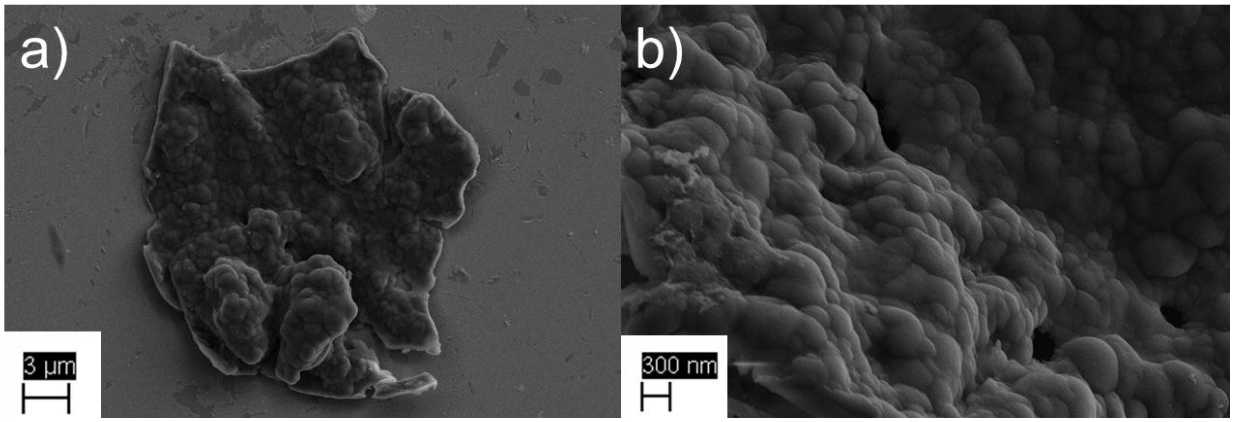

Figure S4: a) SEM images 0f CTF-IP10 and b) zoomed view of CTF-IP10.

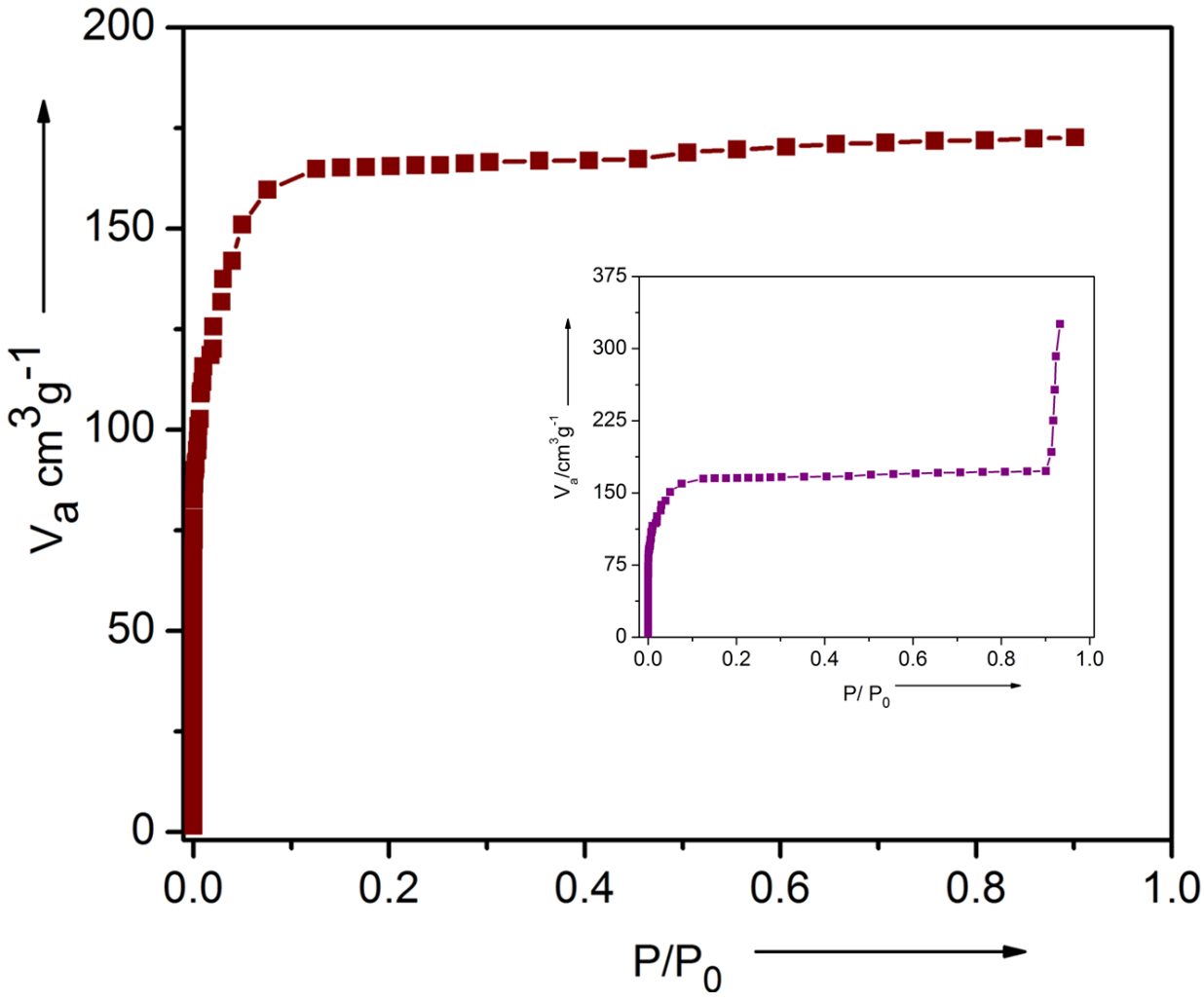

Figure S5: Nitrogen adsorption isotherm of CTF-IP10 at 77K.

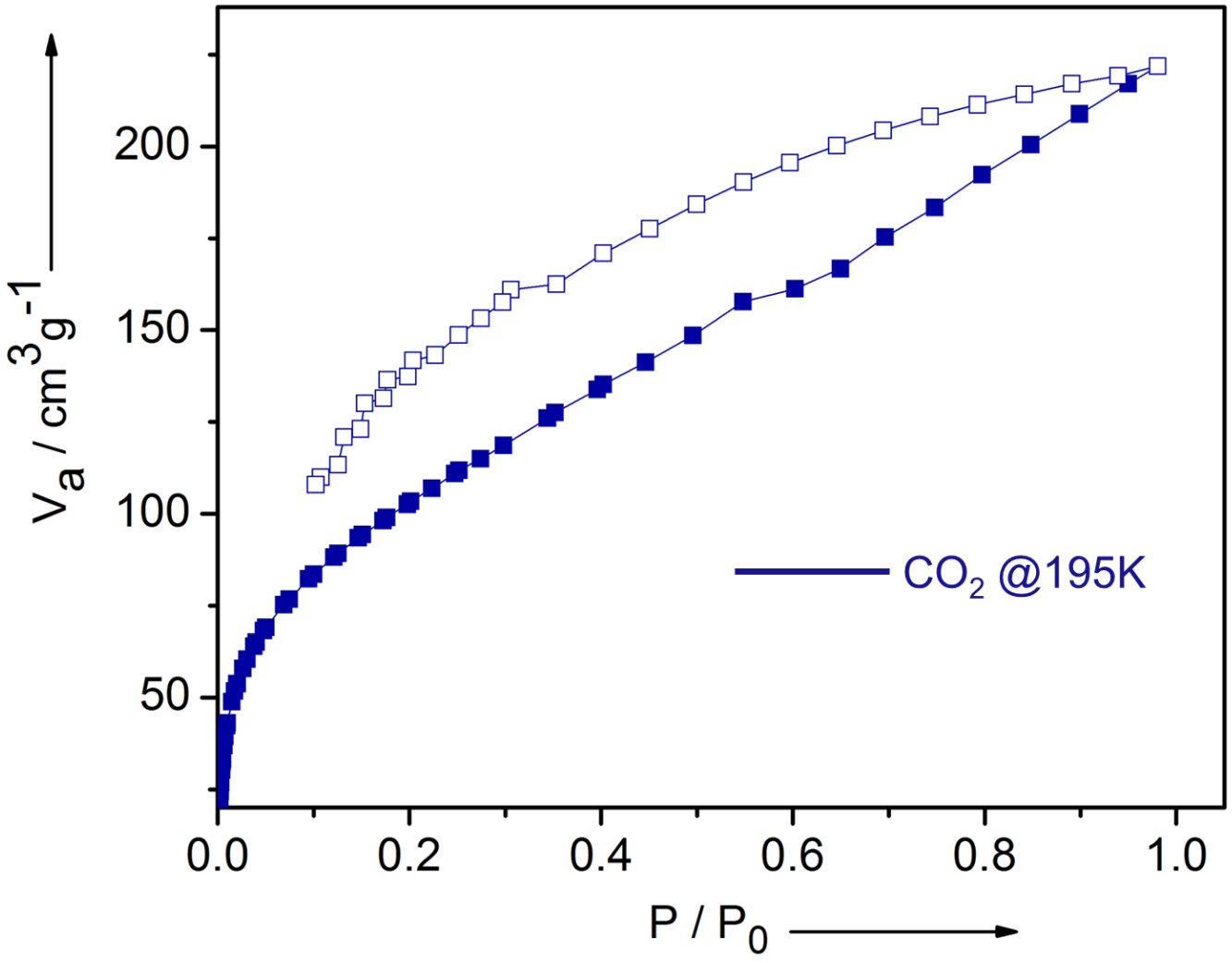

Figure S6: Carbon dioxide adsorption isotherm of CTF-IP10 at 195K.

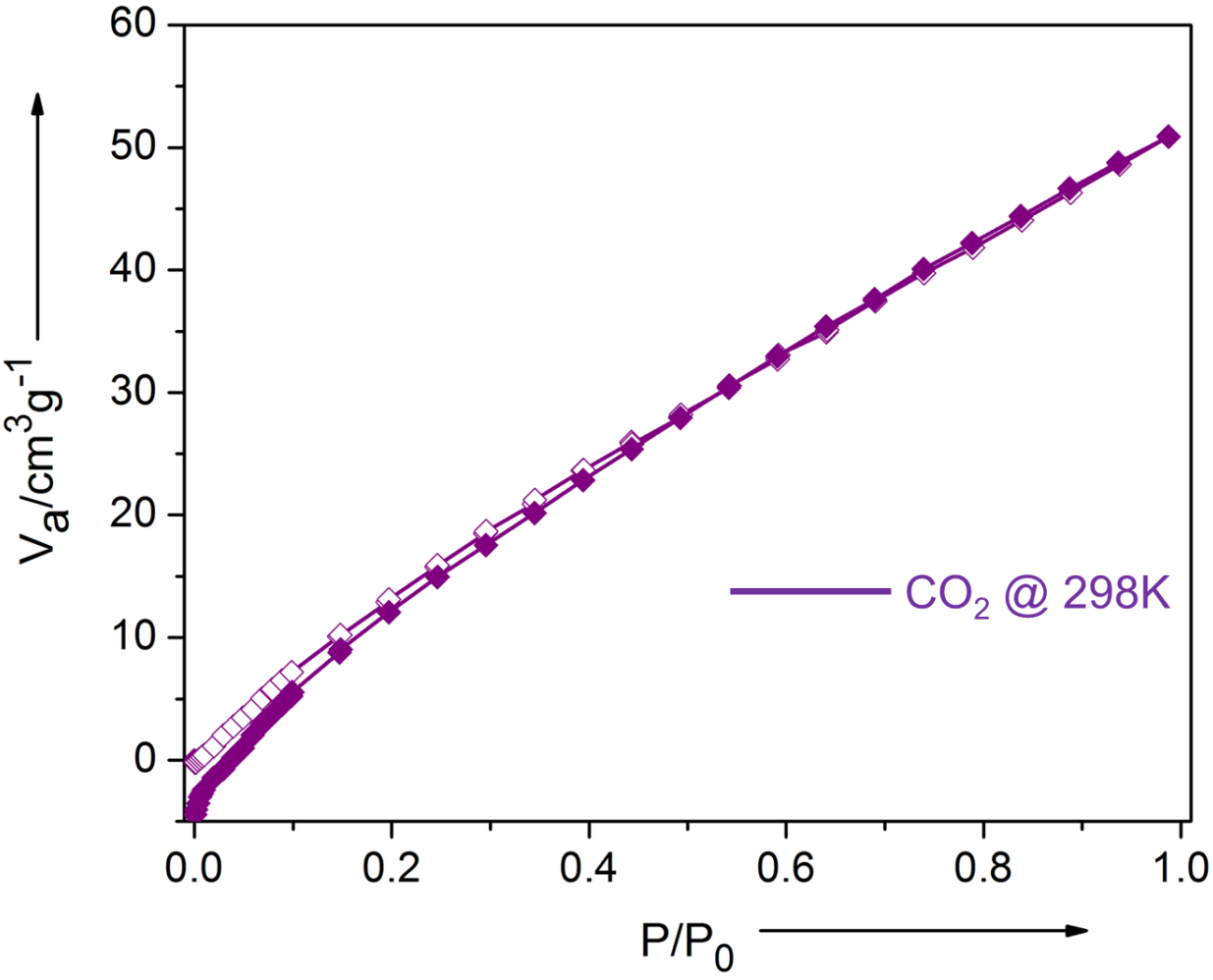

Figure S7: Carbon dioxide adsorption isotherm of CTF-IP10 at 298K.

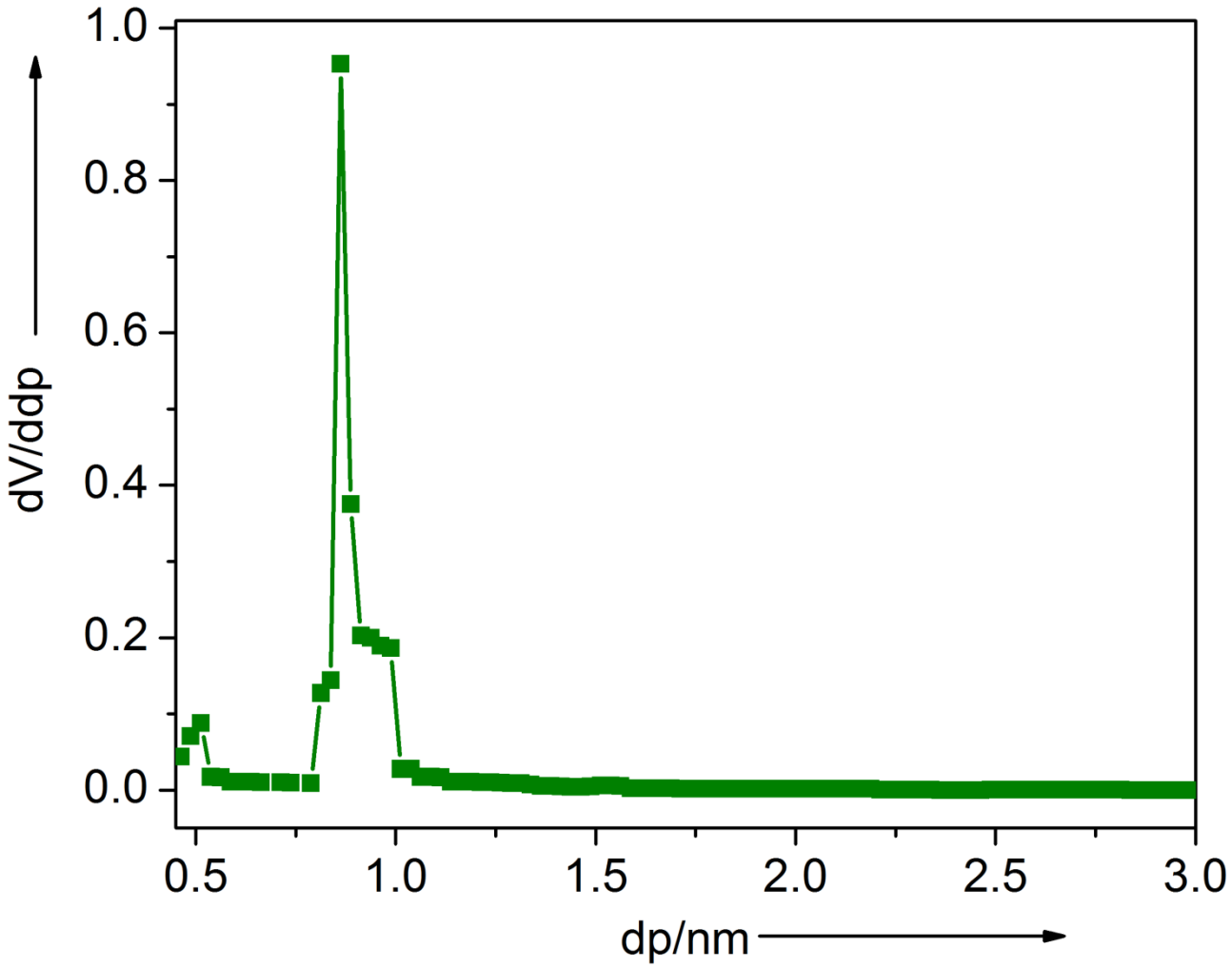

Figure S8: Pore size distribution curve of CTF-IP10.

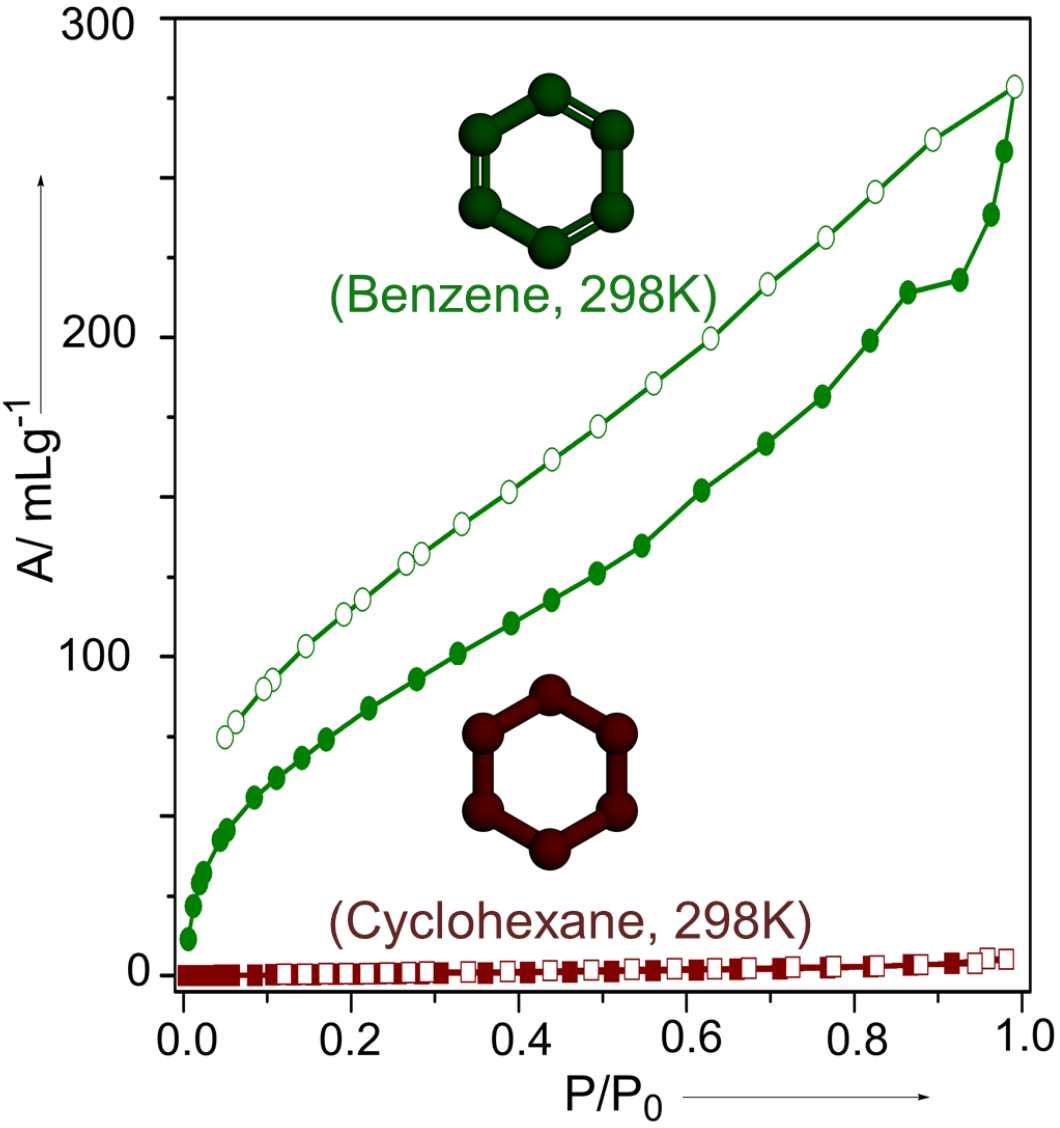

Figure S9: Benzene/Cyclohexane separation by CTF-IP10 at 298K.

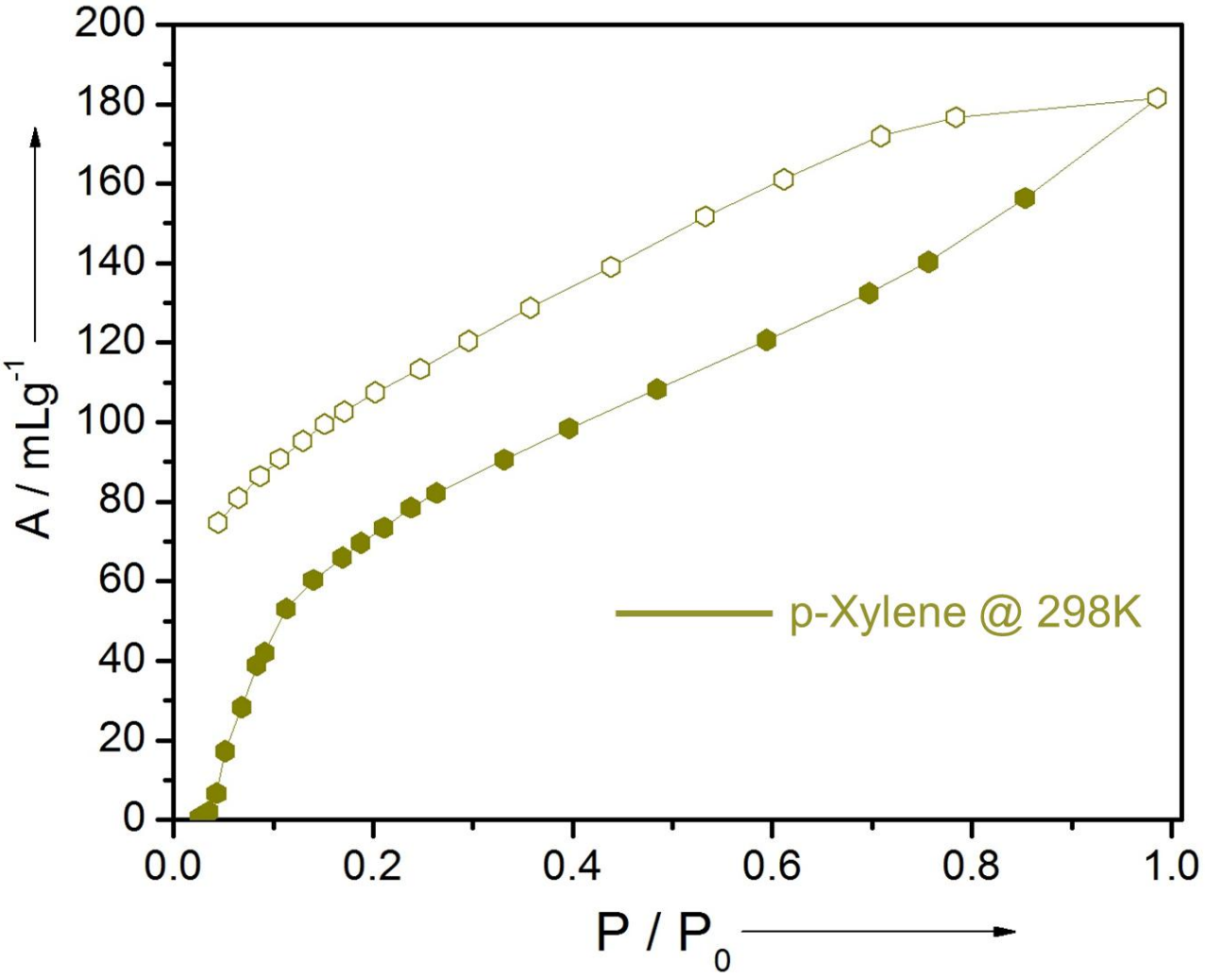

Figure S10: p-Xylene adsorption by CTF-IP10 at 298K.

C_6Cyclic Adsorptive	Boiling and Freezing Points		Conformers
	B.P.	**F.P.**	**Type(s)**
Benzene	353.3 K	278.7 K	Planar
Cyclohexane	353.9 K	279.6 K	Non-planar: Boat and Chair

Table S1. Physical Properties of C_6cyclic adsorptive species.

	Site A			Site B		
	$q_{i,A,sat}$ mol kg^{-1}	$b_{i,A}$ $Pa^{-\nu_{iA}}$	$\nu_{i,A}$ dimensionless	$q_{i,B,sat}$ mol kg^{-1}	$b_{i,B}$ $Pa^{-\nu_{iA}}$	$\nu_{i,B}$ dimensionless
benzene	12	1.94×10^{-12}	2.9	4	1.88×10^{-3}	1
cyclohexane	0.26	7.64×10^{-7}	1.47	3	1.29×10^{-37}	8.7

Table S2. Dual-site Langmuir-Freundlich parameters for aromatic hydrocarbons at 298 K in CTFIP-10.

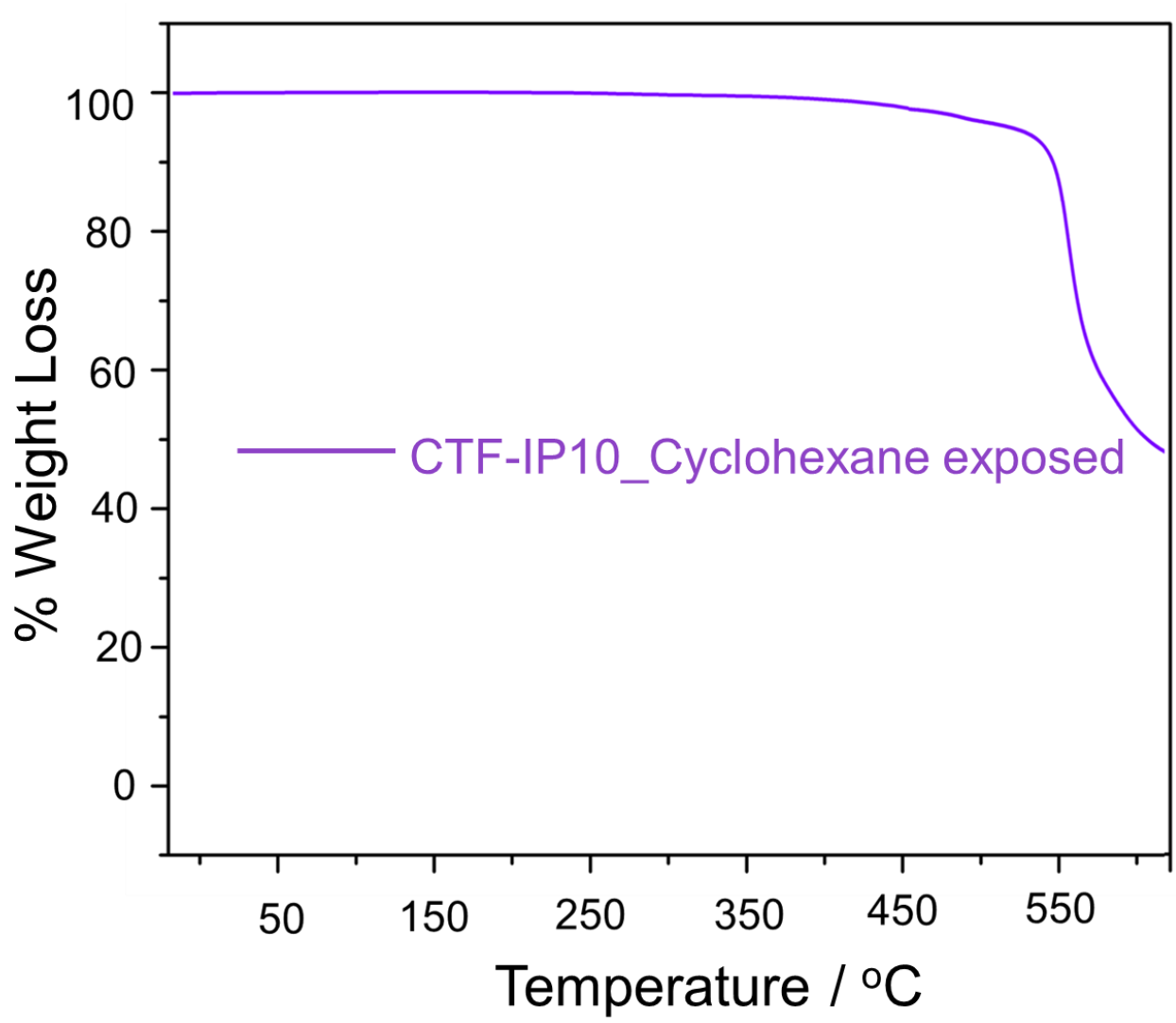

Figure S11: TGA plot of pure cyclohexane vapour exposed compound in desolvated phase of CTF-IP10.

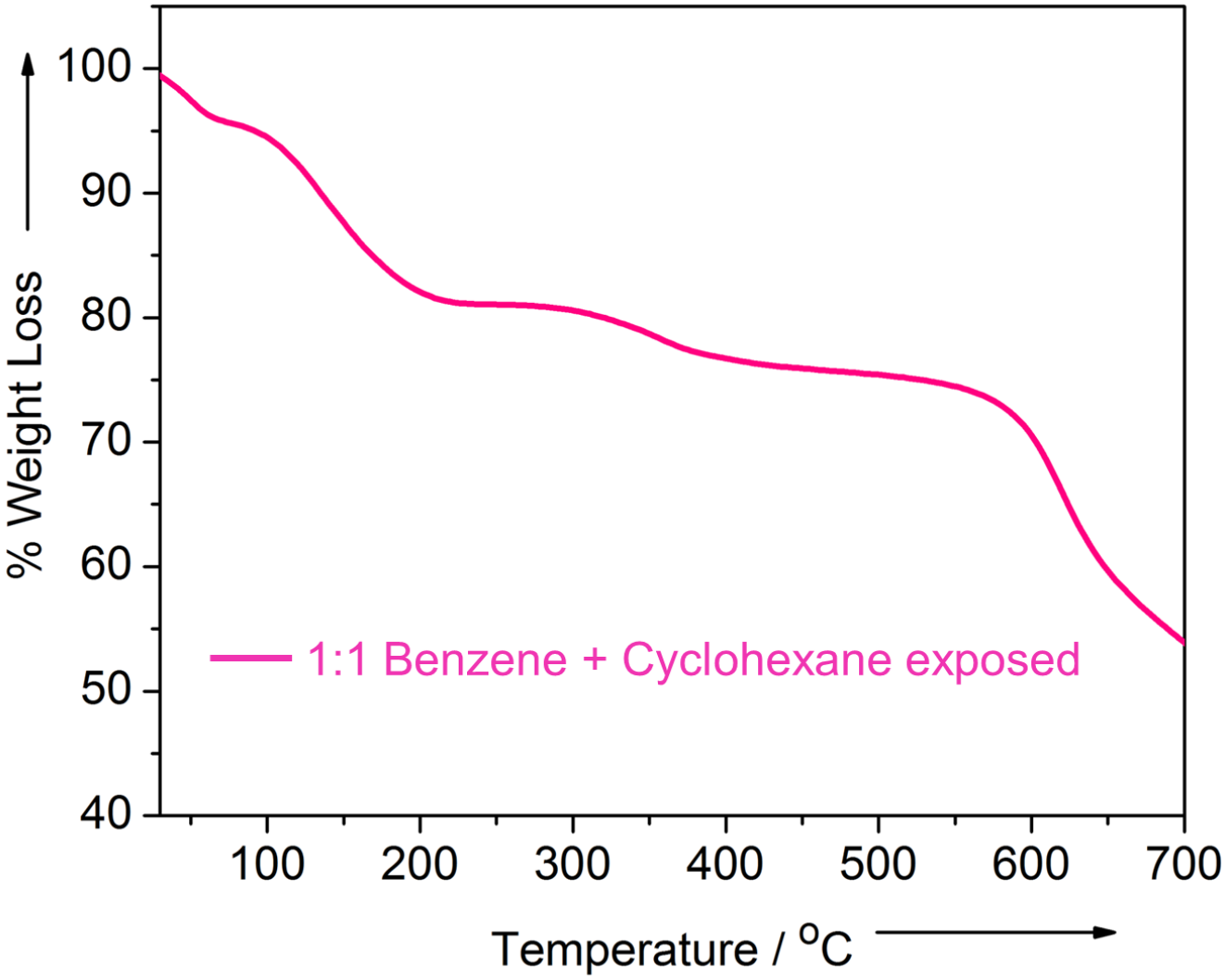

Figure S12: TGA plot of 1:1 mixture of By/Cy vapour exposed compound in desolvated phase of CTF-IP10.

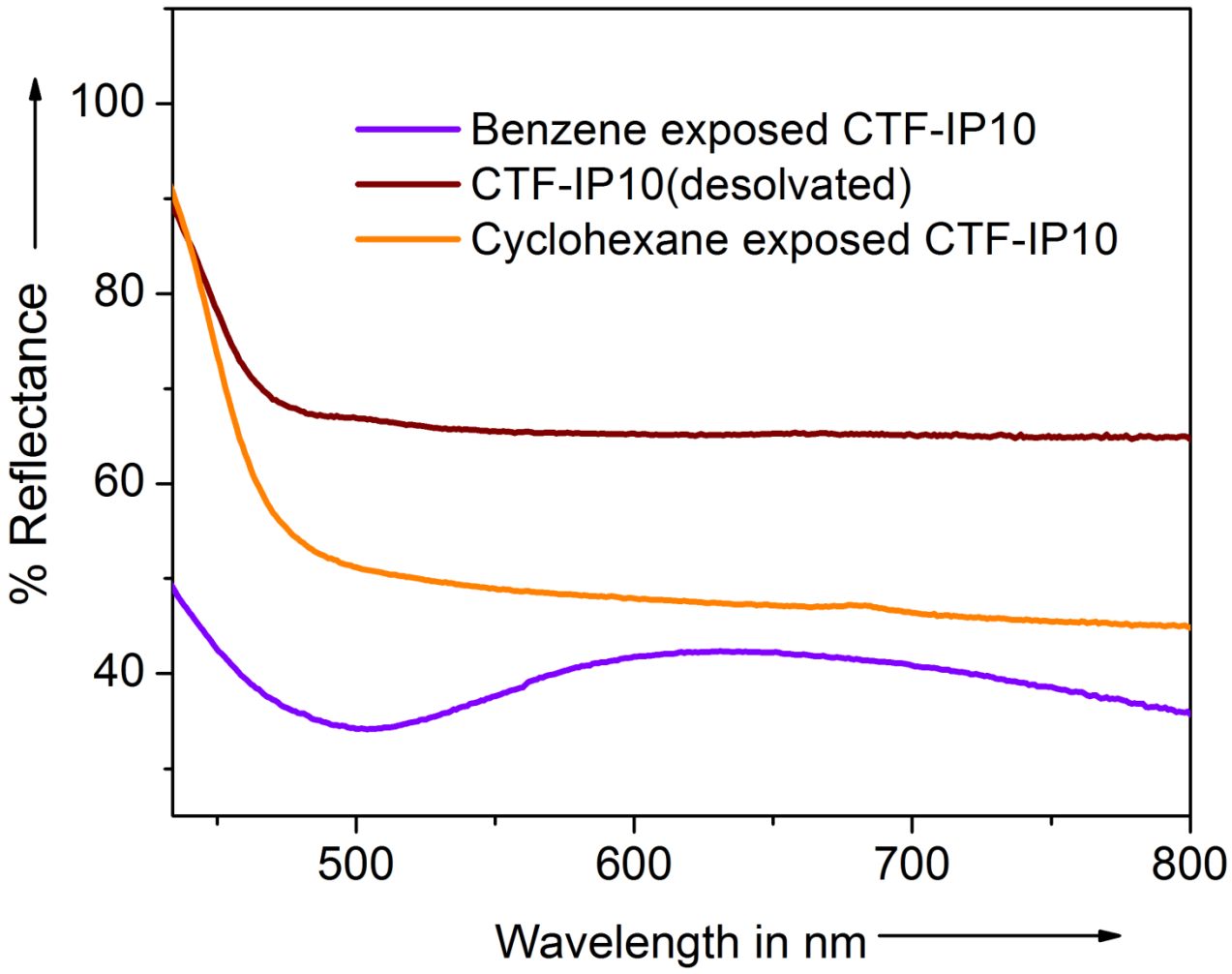

Figure S13: UV spectra of desolvated CTF-IP10 (wine red), Cyclohexane exposed (orange) and Benzene exposed (Violet) CTF-IP10 compounds.

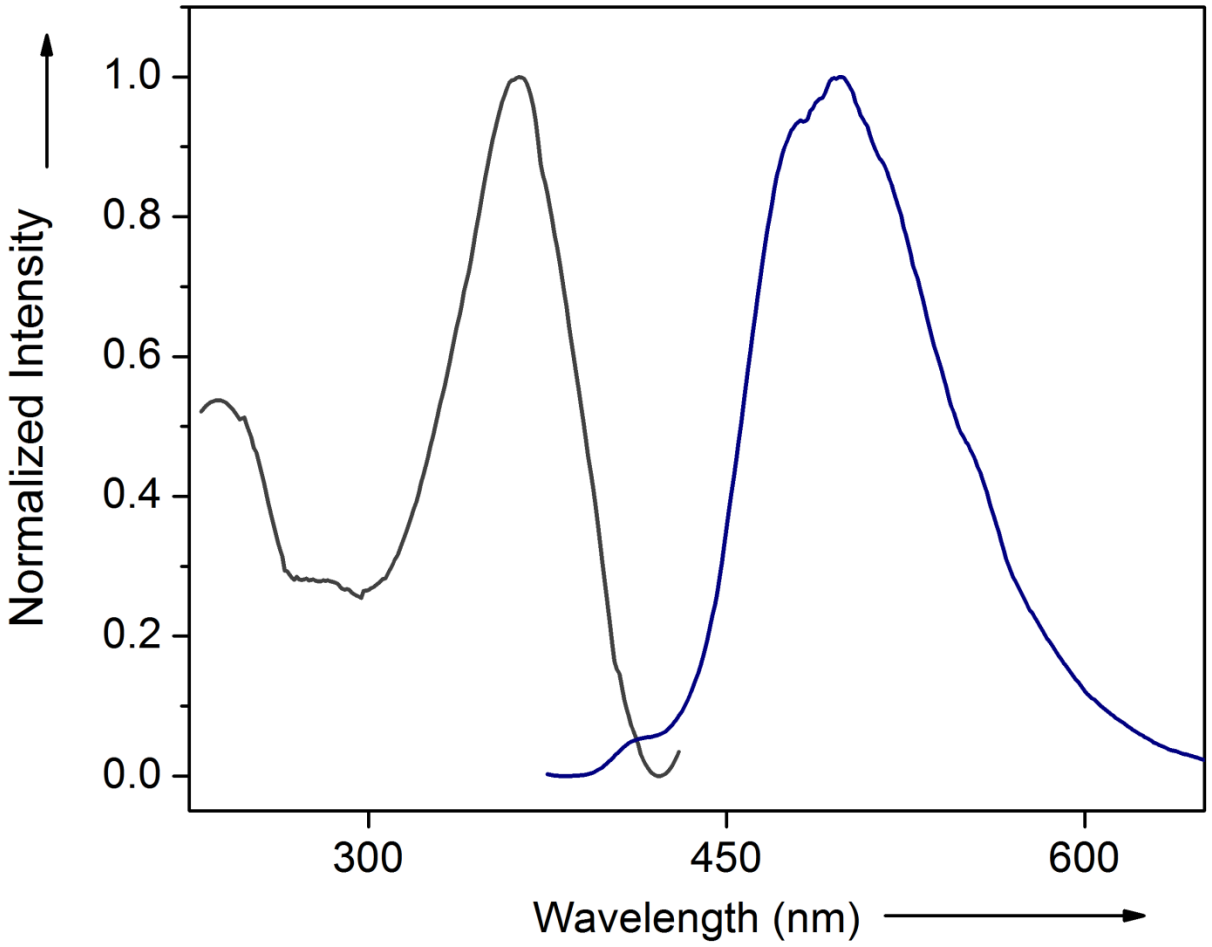

Figure S14: Excitation spectra (grey) and emission spectra (blue) of CTF-IP10.

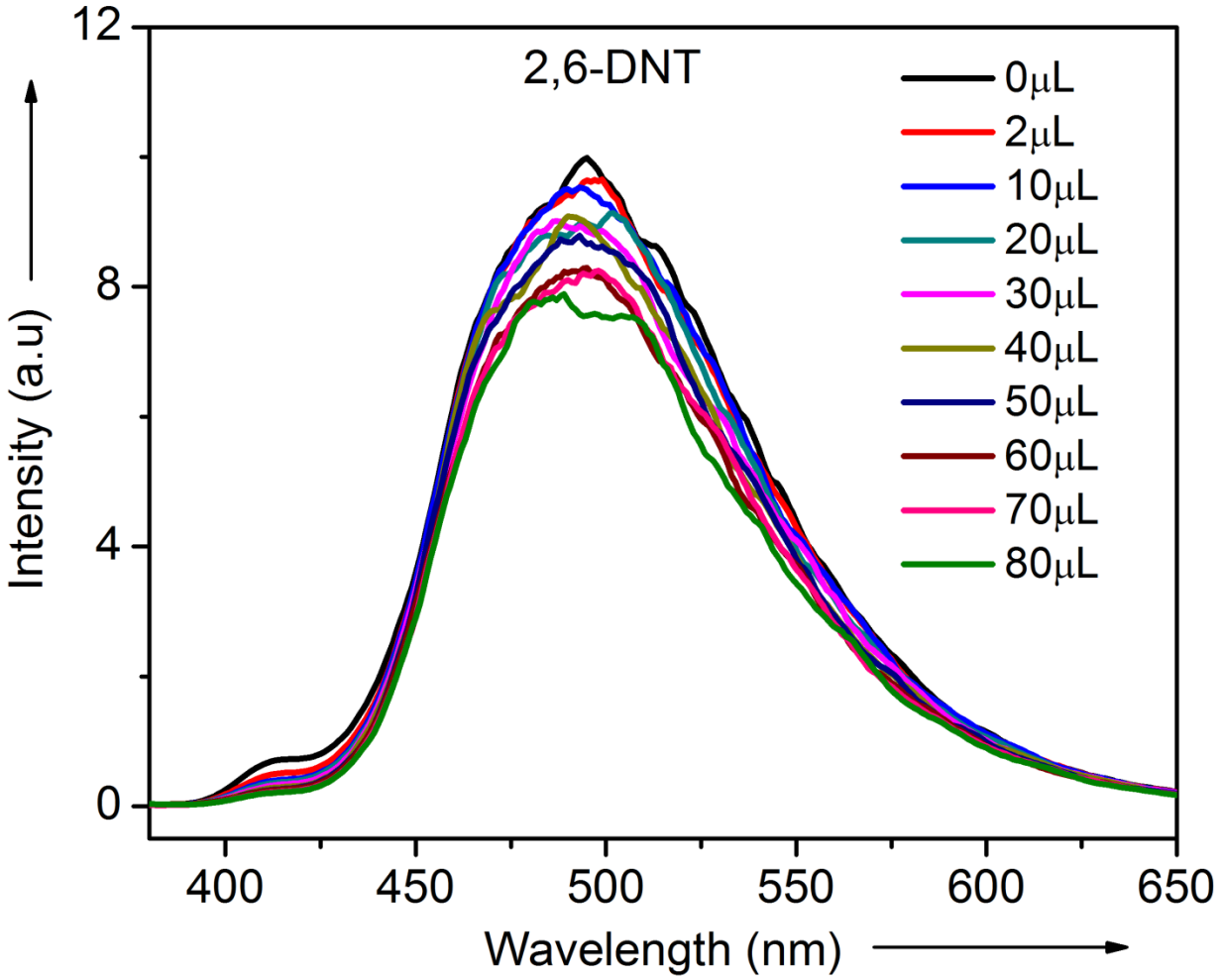

Figure S15: Fluorescence response of CTF-IP10 upon incremental addition of 2,6-DNT.

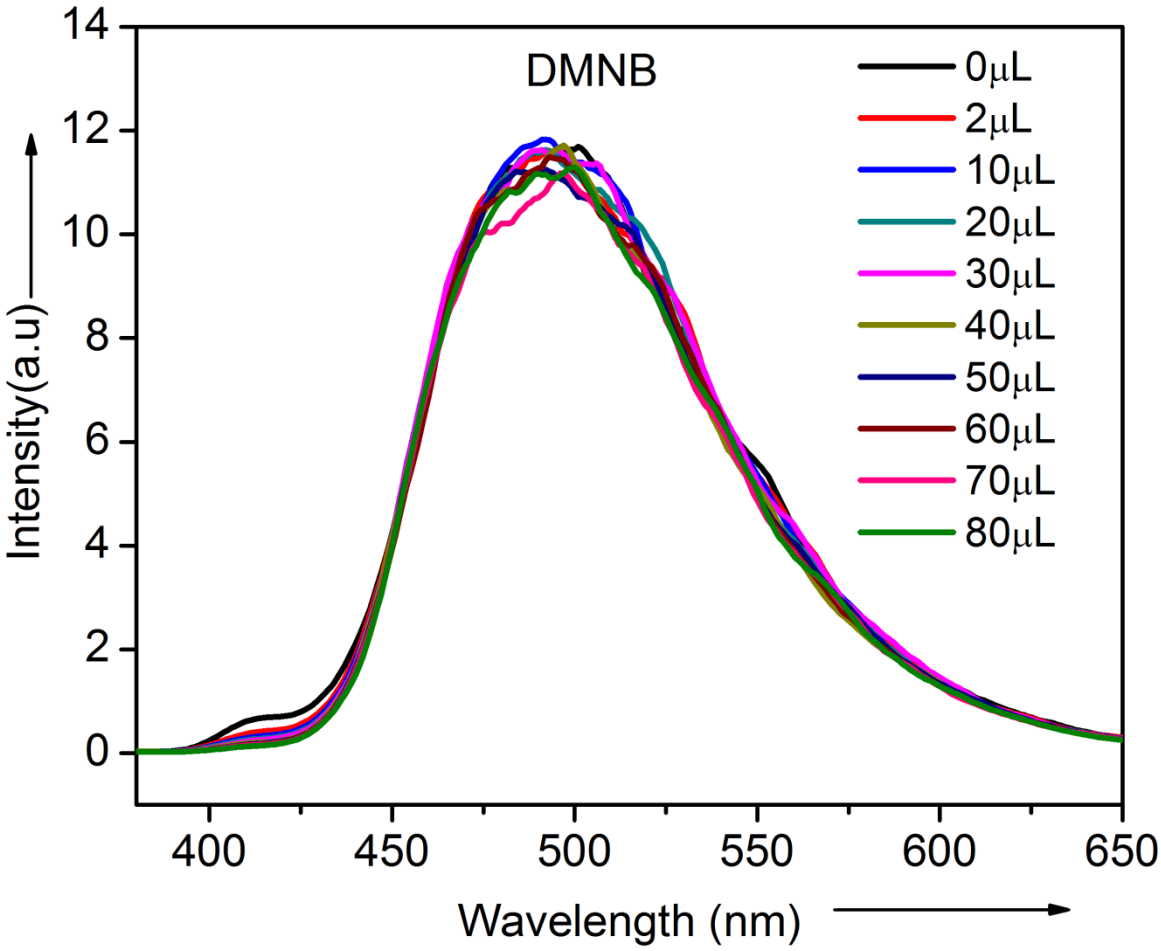

Figure S16: Fluorescence response of CTF-IP10 upon incremental addition of DMNB.

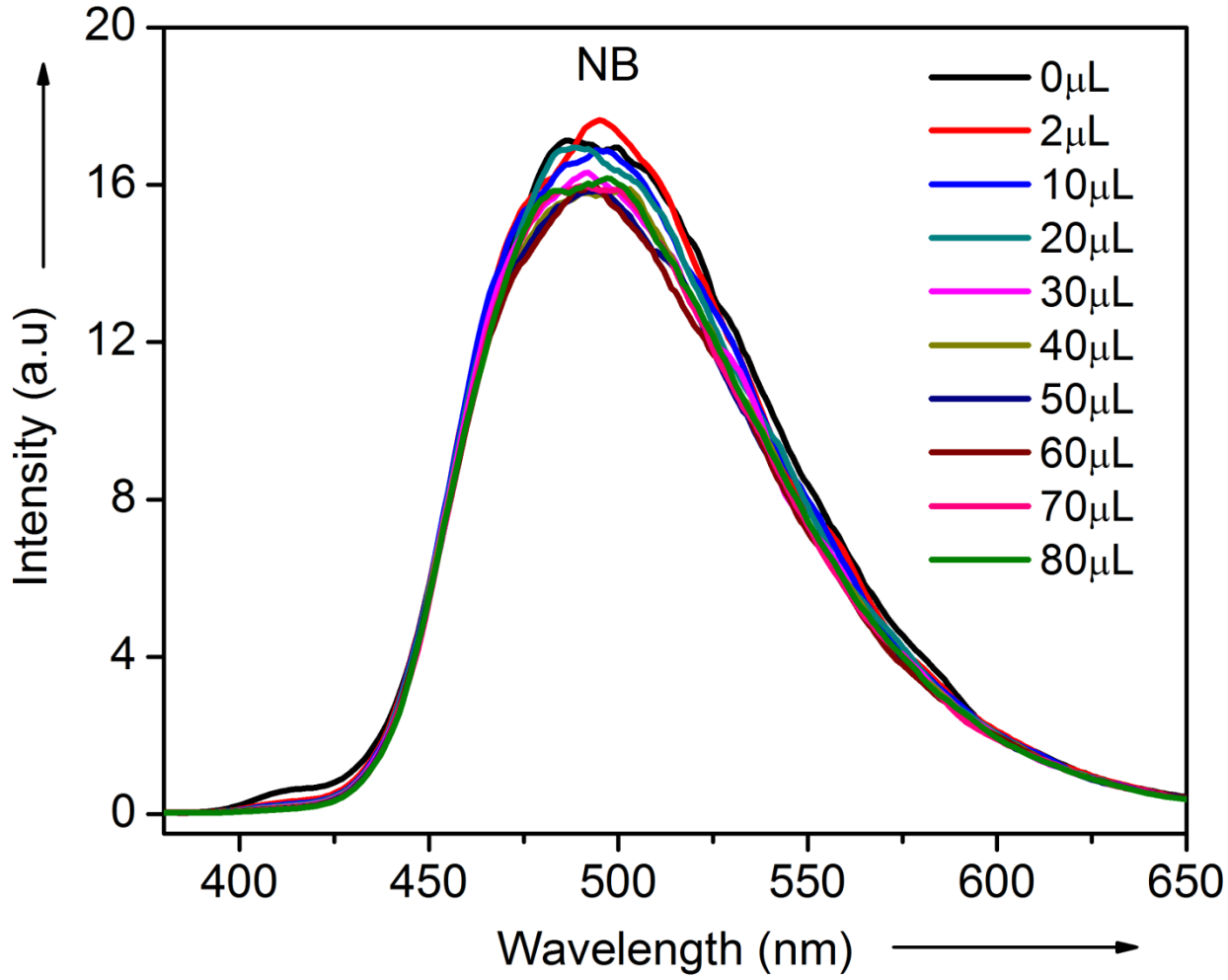

Figure S17: Fluorescence response of CTF-IP10 upon incremental addition of NB.

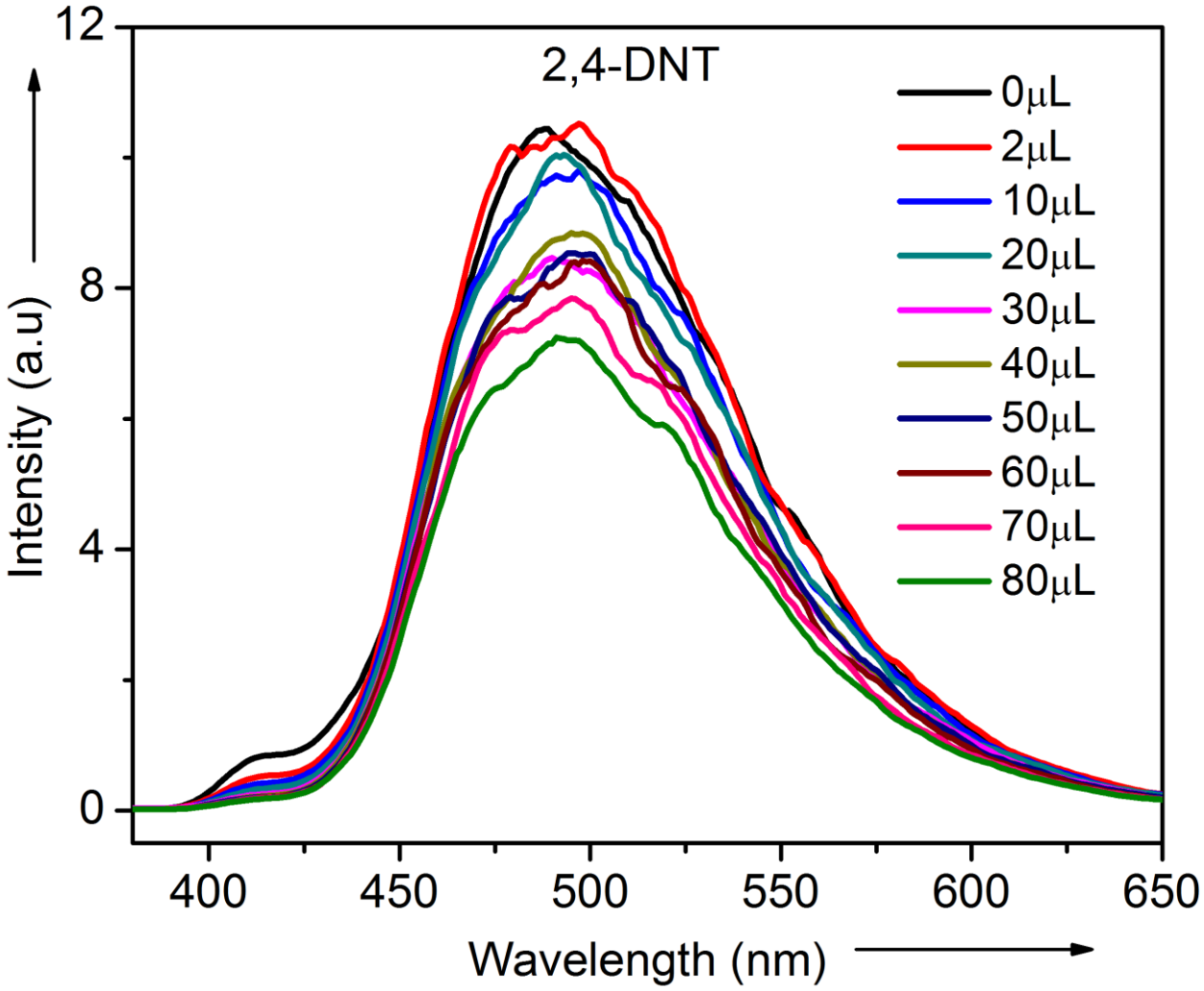

Figure S18: Fluorescence response of CTF-IP10 upon incremental addition of 2,4-DNT.

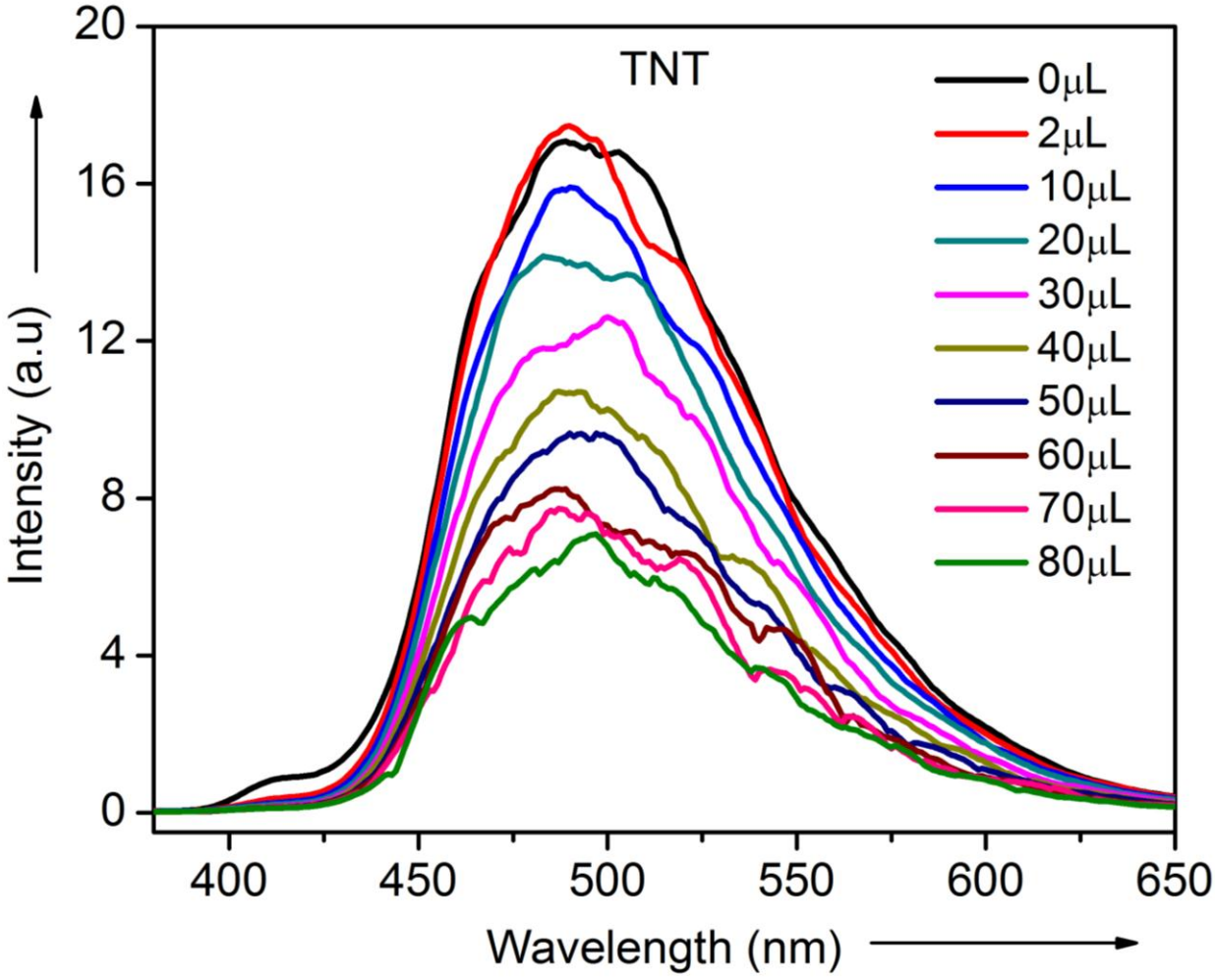

Figure S19: Fluorescence response of CTF-IP10 upon incremental addition of TNT.

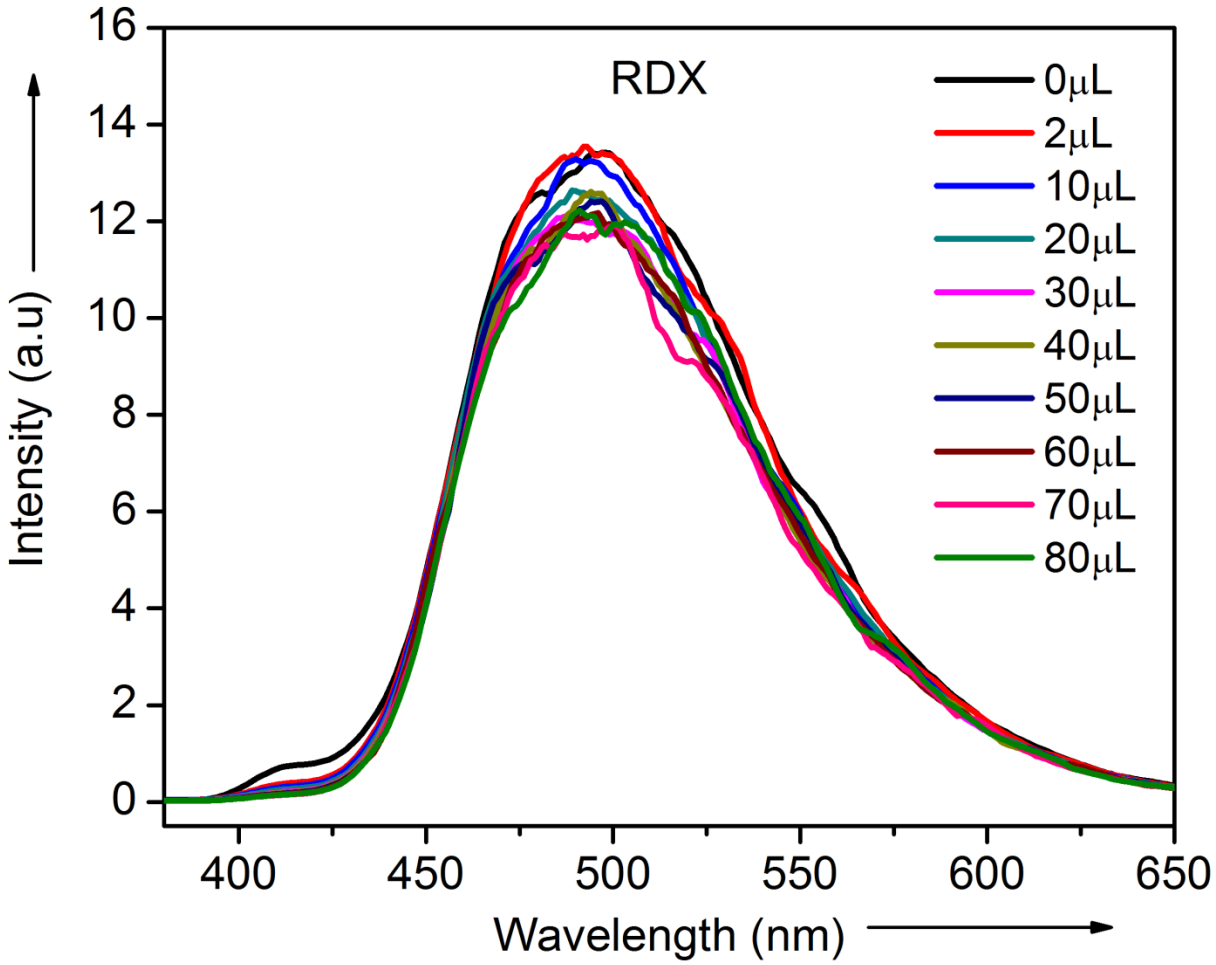

Figure S20: Fluorescence response of CTF-IP10 upon incremental addition of RDX.

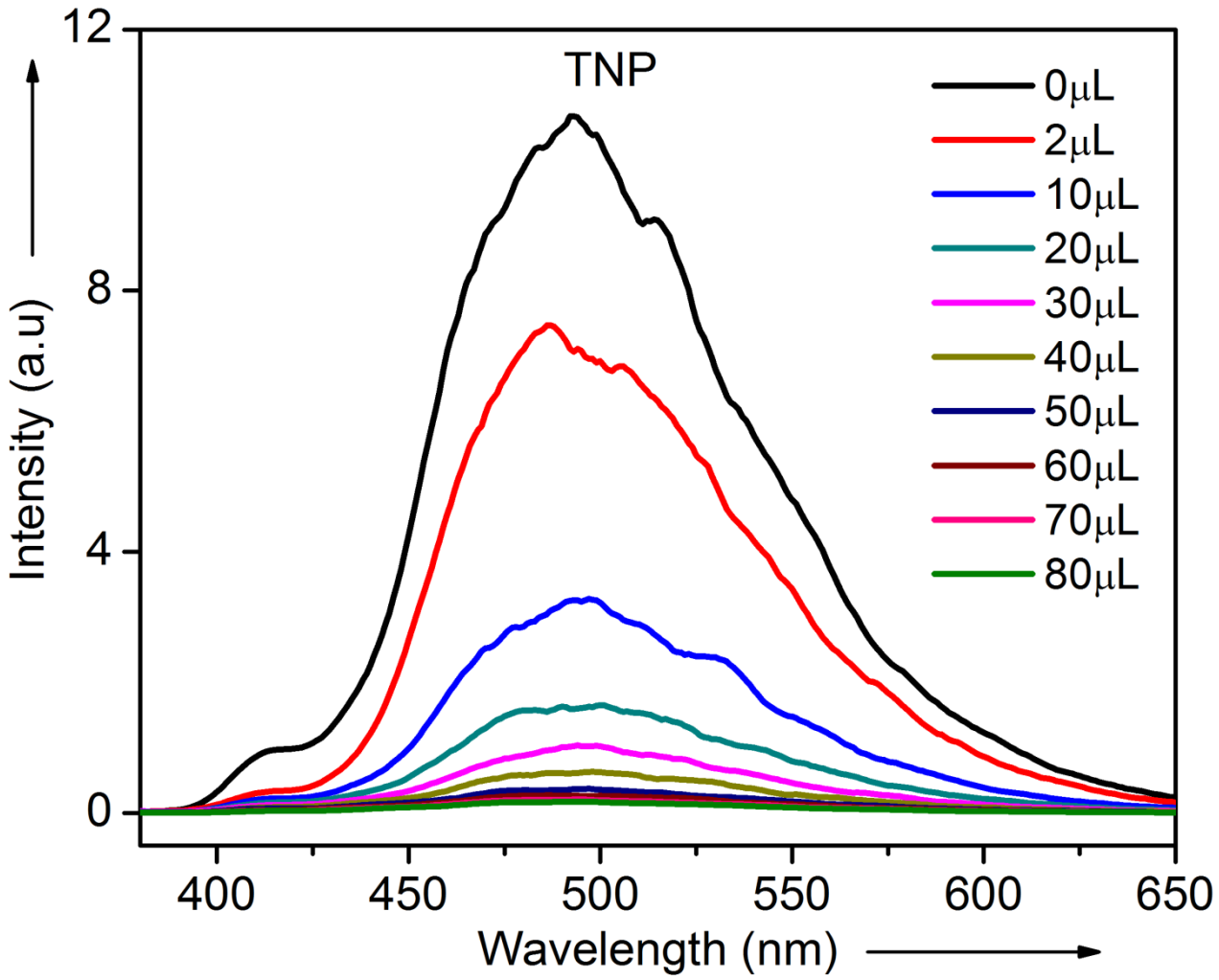

Figure S21: Fluorescence response of CTF-IP10 upon incremental addition of TNP.

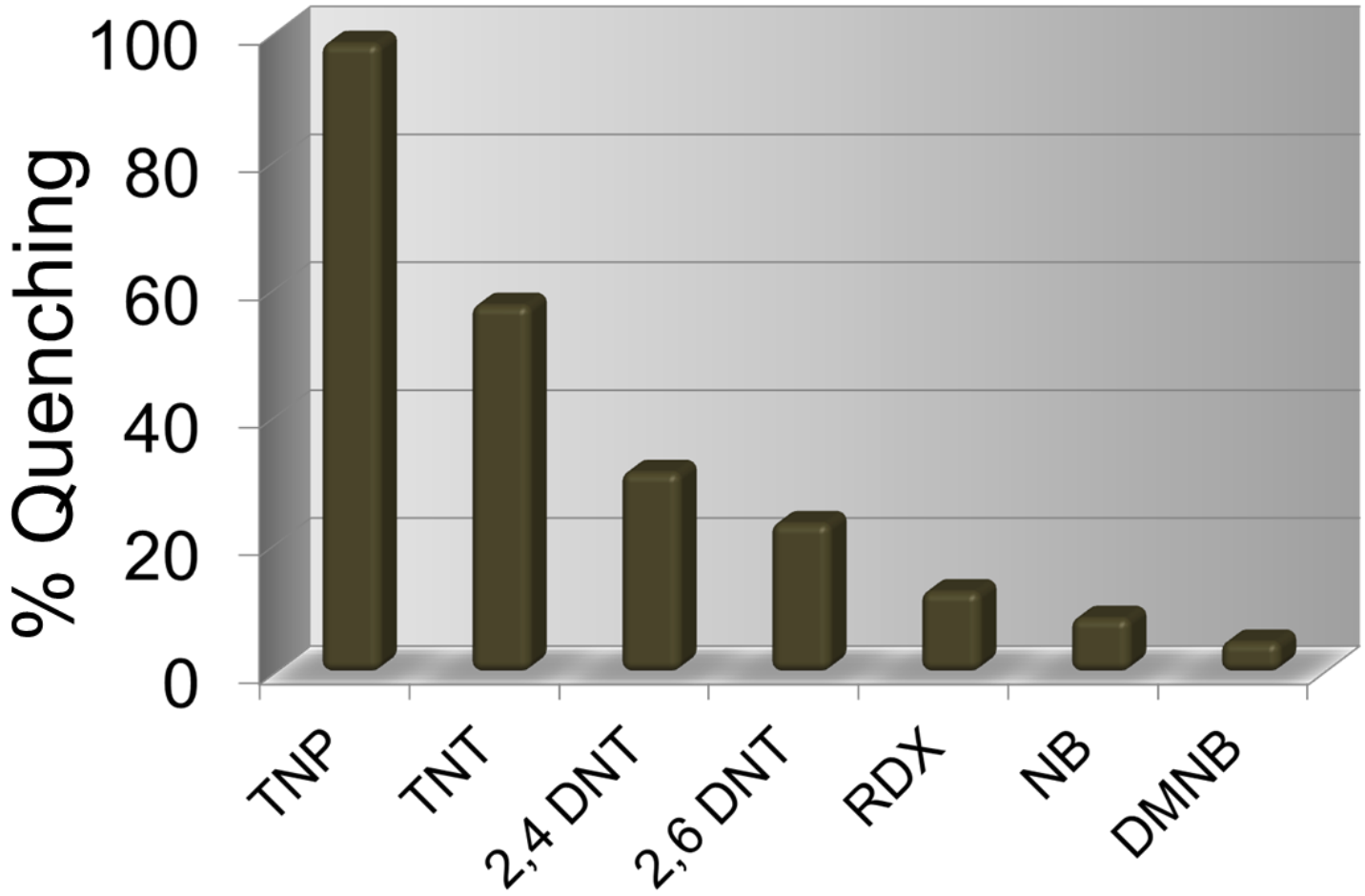

Figure S22: Quenching efficiency in % of TNP and other nitroanalytes

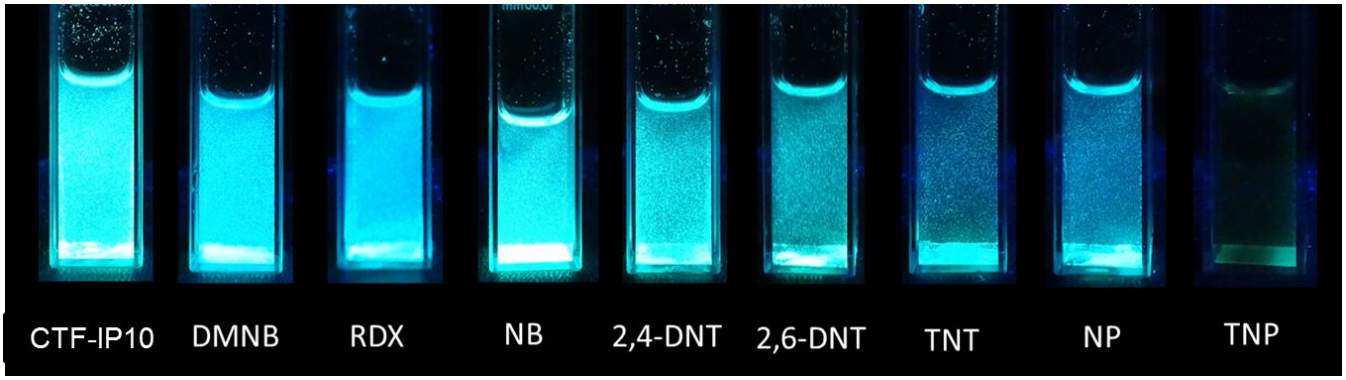

Figure S23: Fluorescence response under UV light of CTF-IP 10 and upon addition of various nitroanalytes to it, showing maximum quenching upon TNP addition.

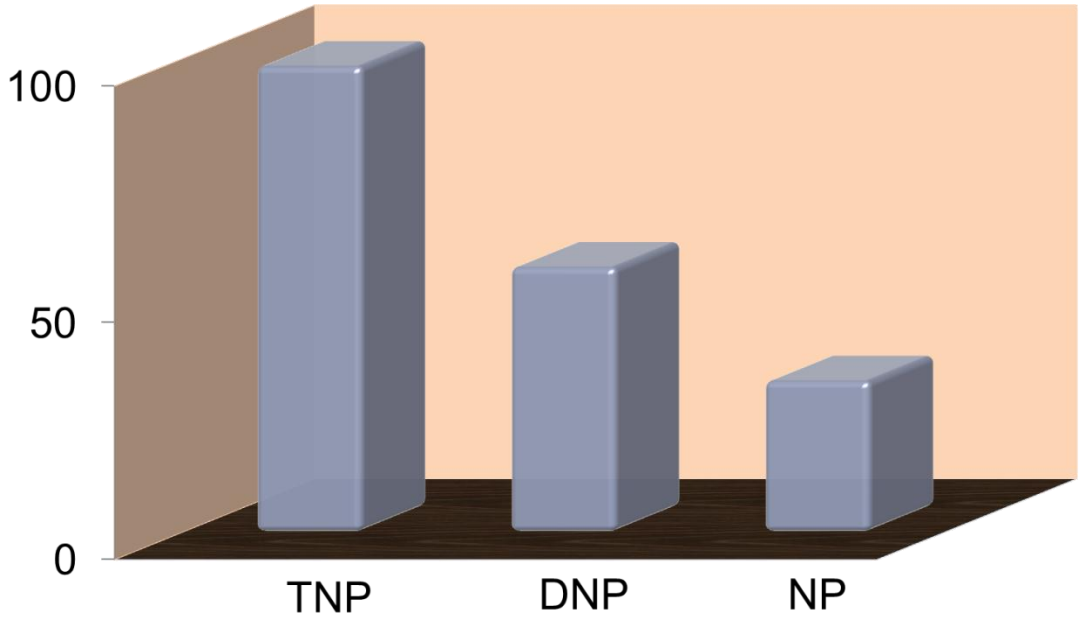

Figure S24: Fluorescence quenching response of CTF-IP10 TNP, DNP and NP.

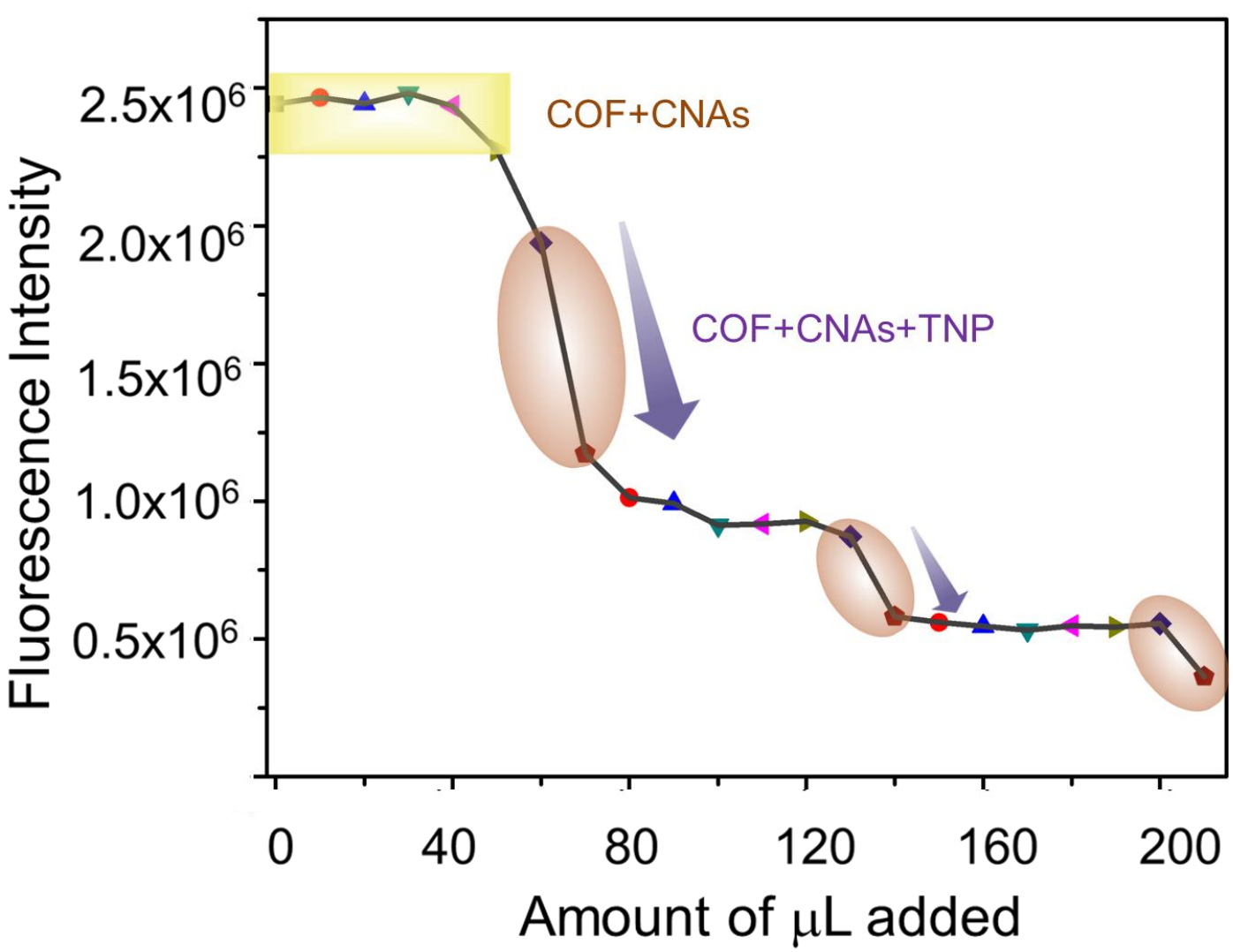

Figure S25: Competitive assay profile showing efficiency of quenching by TNP in presence of other nitro analytes on CTF-IP10

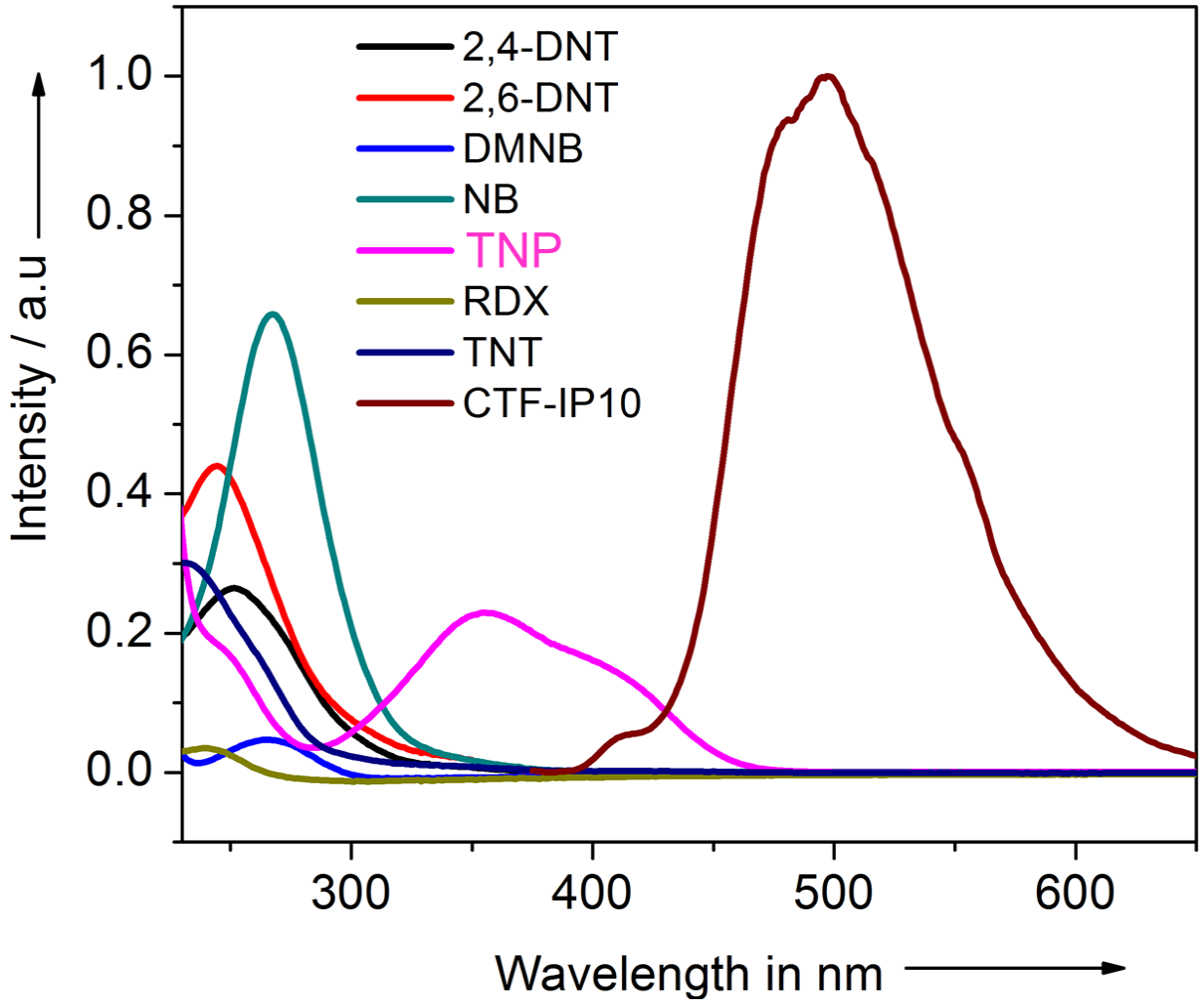

Figure S26: Overlap diagram of the absorption profile of the nitro analytes with the emission profile of CTF-IP10 showing maximum overlap of the absorption TNP with the emission profile of CTF-IP10.

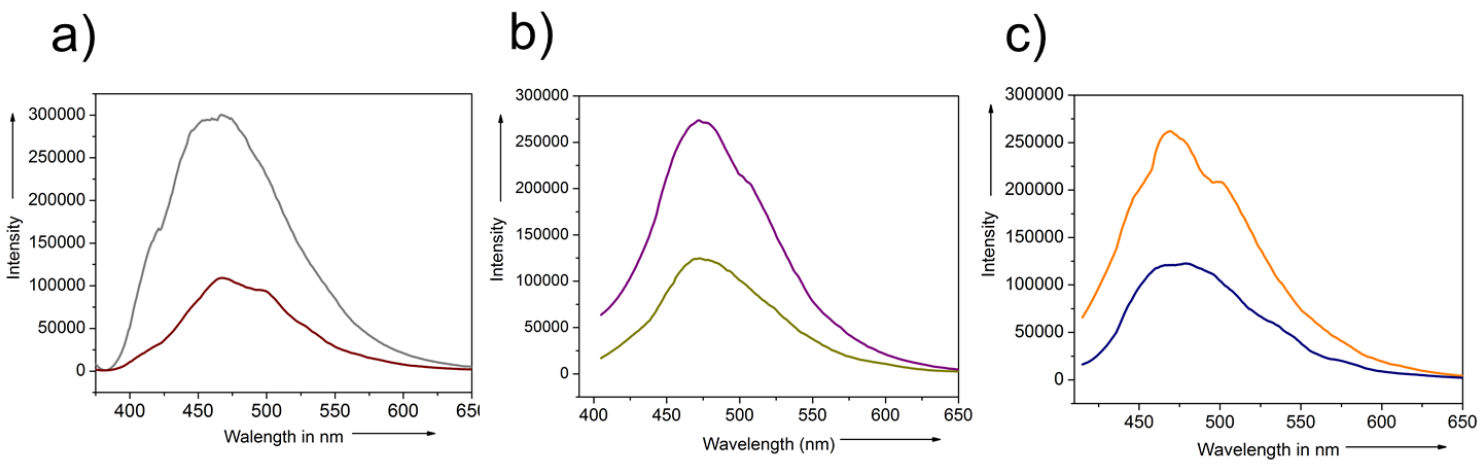

Figure S27: Changes in Fluorescence Intensity of CTF-IP10 upon addition of aqueous TNP soln. 1mmol in H_2O (excited at a. 360nm, b. 390nm and c. 400nm)